SURFACE ACOUSTIC WAVE (SAW) DELAY LINES & RFID ON SILICON/ ALUMINIUM NITRIDE

By

MOHAMED FAWZY MOHAMED IBRAHIM ELBADWY

FINAL PROJECT REPORT

Submitted to the Electrical & Electronics Engineering Programme
in Partial Fulfillment of the Requirements
for the Degree
Bachelor of Engineering (Hons)
(Electrical & Electronics Engineering)

Universiti Teknologi Petronas
Bandar Seri Iskandar
31750 Tronoh
Perak Darul Ridzuan

CERTIFICATION OF APPROVAL

SURFACE ACOUSTIC WAVE (SAW) DELAY LINES & RFID ON SILICON/ ALUMINIUM NITRIDE

by

Mohamed Fawzy Mohamed Ibrahim Elbadwy

A project dissertation submitted to the
Electrical & Electronics Engineering Programme
Universiti Teknologi PETRONAS
in partial fulfilment of the requirement for the
Bachelor of Engineering (Hons)
(Electrical & Electronics Engineering)

Approved:

____

AP.Dr. Varun Jeoti
Project Supervisor

UNIVERSITI TEKNOLOGI PETRONAS
TRONOH, PERAK

September 2014

CERTIFICATION OF ORIGINALITY

This is to certify that I am responsible for the work submitted in this project, that the original work is my own except as specified in the references and acknowledgements, and that the original work contained herein have not been undertaken or done by unspecified sources or persons.

Mohamed Fawzy Mohamed Ibrahim Elbadwy

ABSTRACT

Surface Acoustic Wave (SAW) devices exploit the principle of transducing radio frequency waves into mechanical sound waves propagating across surface of piezoelectric material. These mechanical waves are generated, detected, or reflected by set of metal electrodes. Physical phenomena or unique identification code information can be extracted from the measured /reflected waves based on its different properties such as time delay, phase change or frequency change. Radio identification code implementation methods as well as simulation of SAW device are reviewed in this report. Time pulse position coding is chosen because it provides less sensitivity to variations in temperature and SAW wave velocity. In addition, it is straightforward to implement and simplifies the reader design. To successfully implement the device, proper modeling and simulation is carried out to extract device physical and response parameters such as centre frequency, finger pairs' number, spacing, scattering parameters and frequency response of the system. The equivalent circuit model is used in this study due to faster simulation speed and efficiency.

Aluminum nitride (AlN) is chosen as piezoelectric material due to its high SAW velocity speed, higher coupling factor, cheaper fabrication cost and its chemical characteristics close to that of Silicon Non-reactive with normal semiconductor process chemicals and gases. Data processing and analysis is performed on SAW delay lines implemented on Aluminum nitride to extract device characteristics such as surface acoustic wave velocity, coupling coefficient and center resonance frequency.

.

TABLE OF CONTENTS

LIST OF TABLES

LIST OF EQUATIONS

LIST OF FIGURES

LIST OF ABBREVIATIONS

COM: Coupling of Modes.

ECM: Equivalent Circuit Model.

IDT: Inter-digital Transducer

RFID: Radio Frequency Identification

SAW: Surface Acoustic Wave

CHAPTER 1
INTRODUCTION

1.1 Background

Surface acoustic wave devices have been widely used in filters presented mobile phones and TVs[1]. A surface acoustic wave (SAW) device employs an acoustic wave that is guided along the surface of a piezoelectric crystal, in which the stresses and strains of the mechanical wave are coupled to electric fields[2]. The acoustic wave velocity depends largely on elasticity and density of the piezoelectric material and is very sensitive to change of surface layer mechanical parameters (e.g. density). This sensitivity is the reason why SAW devices are so popular as sensor devices [3]. These features enable compact low-loss devices to be developed for electronics applications. Array structures of metal electrodes are implemented to generate, detect, or reflect the generated acoustic waves. This technology has enormous versatility because standard lithographic techniques can be used to fabricate almost arbitrary geometries.[2]

Inter-digital transducer (IDT) is a comb-like structure of metal fingers connected to electric terminals as seen in figure [1] below. These electrodes can be fabricated by various techniques such as lithographic process, metal deposition and lift-off technique. The center resonant frequency is determined by the width and spacing of fingers. The IDT fingers' length affects the IDT's input admittance . The basic IDT concept uses uniform transducer with equal finger lengths.[4]

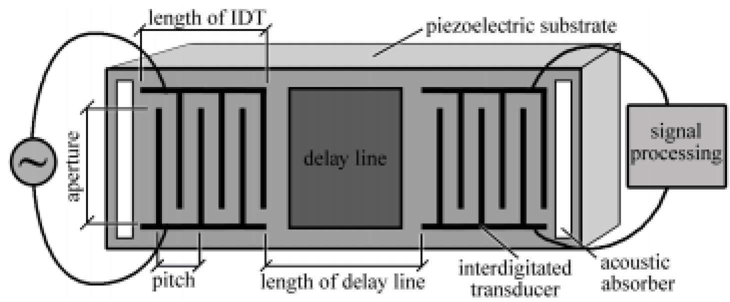

Figure [1]: SAW Delay line structure.

The basic SAW device consists of a piezoelectric material substrate, an input interdigital transducer (IDT) on one side of the surface of the substrate, and a second, output interdigital transducer on the other side of the substrate. delay-line is defined as space between the IDTs, across which the surface acoustic wave will propagate.

As the characteristics of the surface acoustic wave can be affected by the changes in the surface properties as a result of various physical phenomena,SAW sensors can be designed to measure various different phenomena such as gas sensors, humidity and temperature.[4]

RFID is an automatic technology to aid computers or machines to identify objects, record metadata or control individual target through radio waves. it has led to a number of important applications in traffic control, high-value-asset tracking, manufacturing, and most recently supply-chain management.

SAW RFID is a means to implement passive RFID tag nodes that can be wirelessly interrogated. The interrogation signal from the reader is converted to surface acoustic wave (SAW) on the surface of the piezoelectric substrate by means of an interdigital transducer (IDT). By building unique orthogonal ID with the help of set of reflectors, their collision at interrogator is mitigated.

There are different techniques in implementing SAW RFID tag such as Time delay coding (pulse position modulation), resonant coding which contribute to different characteristics of the tag such as range and signal loss, cost, and code dictionary.

The choice of the piezoelectric material and crystal orientation is crucial to achieve desired material properties such as Thermal expansion, electromechanical coupling factor, wave propagation velocity, compatibility with standard microelectronic fabrication techniques, and cost. SAW velocity importance determines the possible frequency range of SAW devices, where an appropriately chosen material may extend the frequency range. Aluminum Nitride (AlN) is chosen as it has good dielectric properties and also shows higher SAW wave velocity thus allowing lower fabrication cost for higher frequency SAW tags [5]. More detailed analysis on AlN is mentioned in literature review.

1.2 Significance of SAW Delay lines & RFID devices

SAW devices such as Delay lines and sensors provide accurate measurements because of sensitivity of SAW to the slightest changes in physical phenomena. SAW devices have the capability of measuring temperature, pressure, strain, torque, and mass-loading. To implement SAW sensor material that undergoes a change in the presence of physical phenomena is to be placed across the delay line. In this way, SAW sensors have wide potential range of applications and can be greatly expanded to include sensing of chemical vapors, biological agents, humidity, light (ultraviolet), and electric and magnetic fields, among other phenomena. The variations in the output signal measured at output IDT are caused by a change in length of the piezoelectric substrate or an increase in mass in the delay line.[4]

The invention of surface acoustic waves RFID has been around for more than 40 years yet it has gained more attention nowadays for numerous reasons.[6] First of all SAW RFID devices are completely passive thus not requiring additional power circuitry. They are immune against harsh environments such as radiation and they have wide range of operating temperature. In addition to that, SAW RFID devices have wider distance range of operation compared to conventional RFID technology.

1.3 Problem Statement

Surface acoustic wave (SAW) Delay lines & RFID is an open and challenging field. Characterization of piezoelectric material is very essential to obtain accurate design parameters such as SAW velocity and Coupling coefficient. Aluminum nitride is not fully characterized yet and needs further investigation to find SAW velocity and coupling coefficient based on piezoelectric layer thickness.

For SAW RFID devices, a compromise between range, signal losses, power consumption, and code dictionary has to be made. Optimal implementation of RFID tag is crucial to increase the range, decrease signal losses as well as increasing data code. Simulation of SAW RFID is required to understand and investigate reaching optimal design.

1.4 Objectives

1. To simulate surface acoustic wave (SAW) IDT structure, Delay line structure and RFID tag using suitable simulation method.
2. To propose a suitable tag encoding technique for a surface acoustic wave (SAW) RFID tag.
3. To investigate and characterize SAW devices on Aluminum nitride (AlN) film.

1.5 Scope of Study

The project is time frame is seven months. In this limited time, the scope of the study is focused onto simulation IDT, SAW delay line/RFID structure using equivalent circuit model, and investigating and extracting Aluminum Nitride SAW velocity and coupling coefficient for SAW delay lines implemented on AlN/SiO2/Si structure.

The feature extraction is achieved by processing scattering parameters of the various delay lines to remove feedthrough and triple time reflection effects to determine the resonant frequency of the device.

Based on centre frequency and design IDT finger width parameter, SAW velocity is calculated. The calculated SAW velocities are compared with expected velocity values extracted from theoretical modeling of the device. The coupling coefficient is calculated using admittance information of the devices and compared with literature reported values.

CHAPTER 2

LITERATURE REVIEW AND THEORY

2.1 Device simulation

The major component of SAW tag is Inter-digital transducer. Normal bidirectional transducer consists of 2 acoustic ports and 1 electric port. To model IDT different approaches can be taken for example:

1. Coupling of modes theory[7, 8].
2. Mason Equivalent circuit model[5].
3. Mixed circuit model[9].
4. Delta function[8].

The equivalent circuit modeling gives the advantage of being fast and does not require heavy computations. It provides designer with basic design parameters such as fingers width, aperture, delay line distance, frequency response, impedance parameters and transfer characteristics of SAW device.

For this section of project Mason equivalent circuit model and COM model is investigated in details. The most important IDT parameters are the centre frequency, finger width, spacing and aperture.

$$f_0 = \frac{v_{saw}}{\lambda}$$

Equation 1 : Device Resonant frequency

$$where\ v_{saw}\ is\ the\ speed\ of\ acoustic\ wave\ across\ the\ surface\ of\ piezolectric\ material,$$
$$and\ \lambda\ is\ the\ wavelength$$

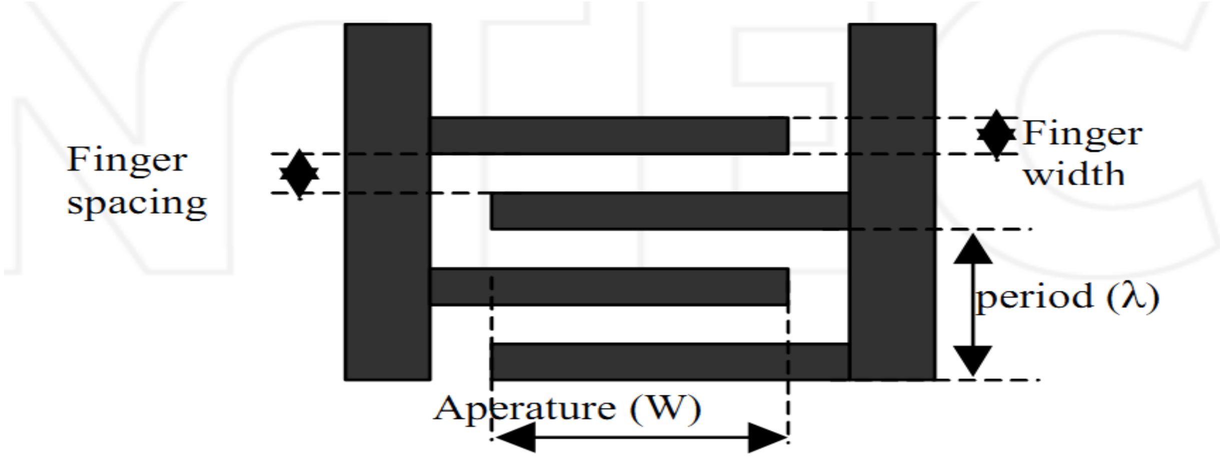

Figure [2] :IDT Physical parameters

Finger width = $p = \lambda/4$

For optimal design, IDT resistance (real impedance) must match the source resistance normally 50 ohm for major test equipments. The IDT finger overlap or aperture height (W) is normally optimized based on the following equation[10]

$$W = \frac{1}{R_{in}}\left(\frac{1}{2 f_0 C_s N_p}\right)\frac{\left(4k^2 N_p\right)}{\left(4k^2 N_p\right)^2 + \pi^2}$$

Equation 2: Aperture governing equation

It is also crucial to investigate insertion loss of SAW device. Insertion loss is function of frequency and the lowest loss appears at $f = f_o$

$$IL(f) = -10\log\left[\frac{2G_a(f)R_g}{\left(1+G_a(f)R_g\right)^2 + \left[R_g\left(2\pi f C_T + B_a(f)\right)\right]^2}\right]$$

Equation 3: Insertion loss

2.1.1 Mason's Equivalent Circuit model (ECM)

Schematic below shows mason's ECM for 1 pair on IDT fingers[5]

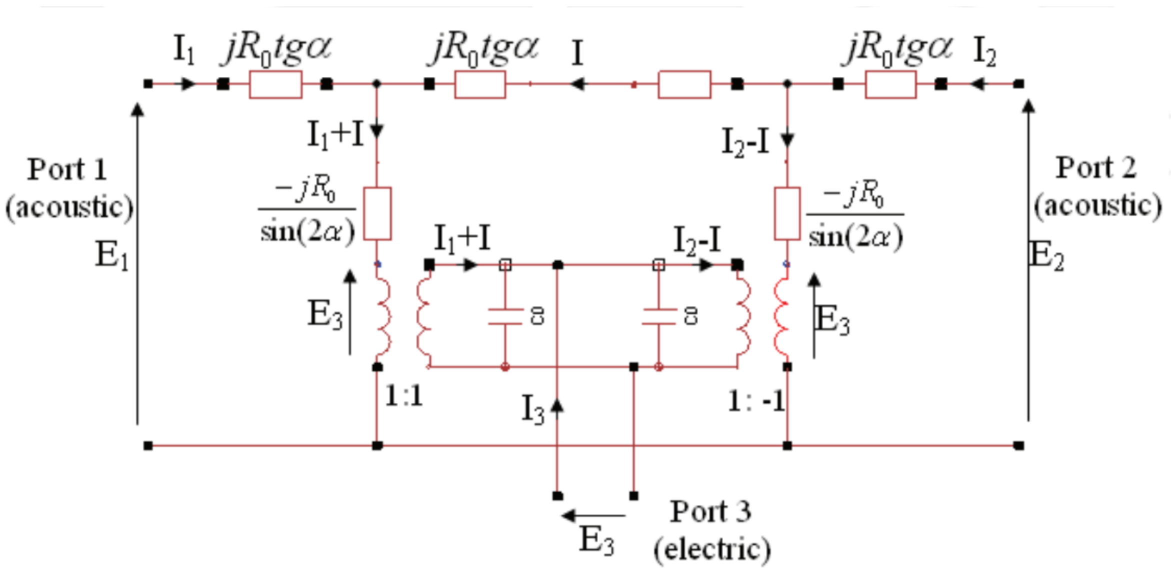

Figure [3]: Mason's ECM for IDT finger pair

$$\alpha = \frac{\pi}{2}\frac{\omega}{\omega_0}$$

$$R_o = \frac{2 * \pi}{\omega_0 * C_s * K^2}$$

Equation 4: Mason's ECM paramters

Where R_o is electrical equivalent of mechanical impedance Z_o ,

K is electromechanical coupling coefficient, C_s : electrode capacitance per section and ω_0 is center angular frequency.

For N number of pairs of IDT the model can be cascaded to represent series of 3 port networks as in figure below[5]

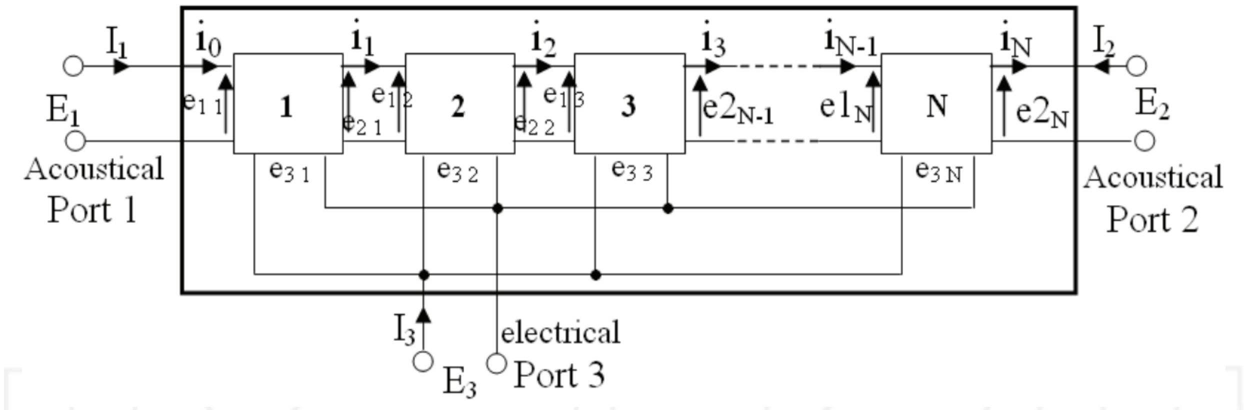

Figure [4]: IDT Equivalent Circuit

The system is represented using admittance matrix of 3 port network

$$\begin{bmatrix} i_1 \\ i_2 \\ i_3 \end{bmatrix} = \begin{bmatrix} y_{11} & y_{12} & y_{13} \\ y_{21} & y_{22} & y_{23} \\ y_{31} & y_{32} & y_{33} \end{bmatrix} \begin{bmatrix} e_1 \\ e_2 \\ e_3 \end{bmatrix}$$

Equation 5: IDT Admittance Matrix

The admittance is calculated by MATLAB equations

```
%-------------------------------------
% Y paramters calculation
Y11=-1i*Go*cot(4*Np*alpha);
Y12=(1i*Go)./(sin(4*Np*alpha));
Y13=-1i*Go*tan(alpha);
Y33=1i*Np*((2*pi*f*Cs)+(4*Go.*tan(alpha)));
%-------------------------------------
Y22=Y11;
Y21=Y12;
Y31=Y13;
Y23=-Y13;
Y32=-Y13;
Y=[Y11 Y12 Y13;Y21 Y22 Y23;Y31 Y32 Y33];
%-------------------------------------------
```

Figure [5]: Code Implementation of Admittance Matrix.

The propagation path equivalent circuit based on mason's model can be represented as follow

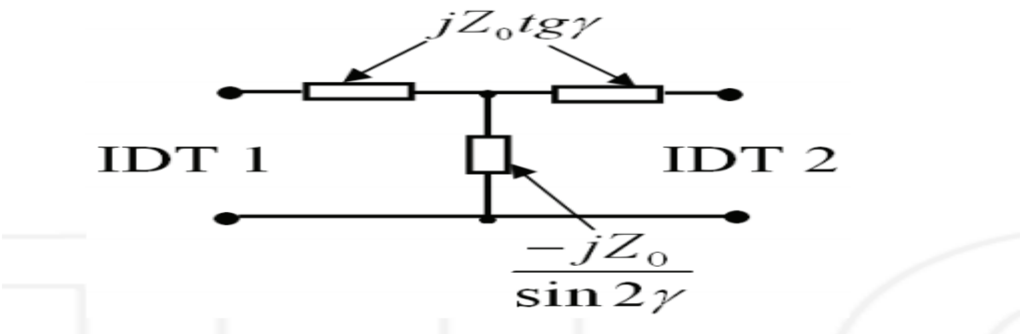

Figure [6]: Propagation Path Equivalent Circuit.

$$Z_0 = \left(\frac{1}{R_0}\right) \ , \gamma = (\omega * l)/(2 * v_{Saw})$$

Equation 6: Propagation Path Equation

Where l is the length of propagation path, usually represented in multiple of wavelengths.

2.1.2 Coupling of Mode Equivalent Circuit Model

The Coupling-Of-Modes is a branch of the theory related to wave propagation in periodic structure. COM theory covers a variety of wave phenomena, including the diffraction of electromagnetic waves on periodic gratings, optical and ultrasonic waves in multi-layered structures, waves and particles in crystals. An excellent recently written review by K.Hashimoto[5] of COM theory used in SAW devices.

The circuit model is shown in figure below

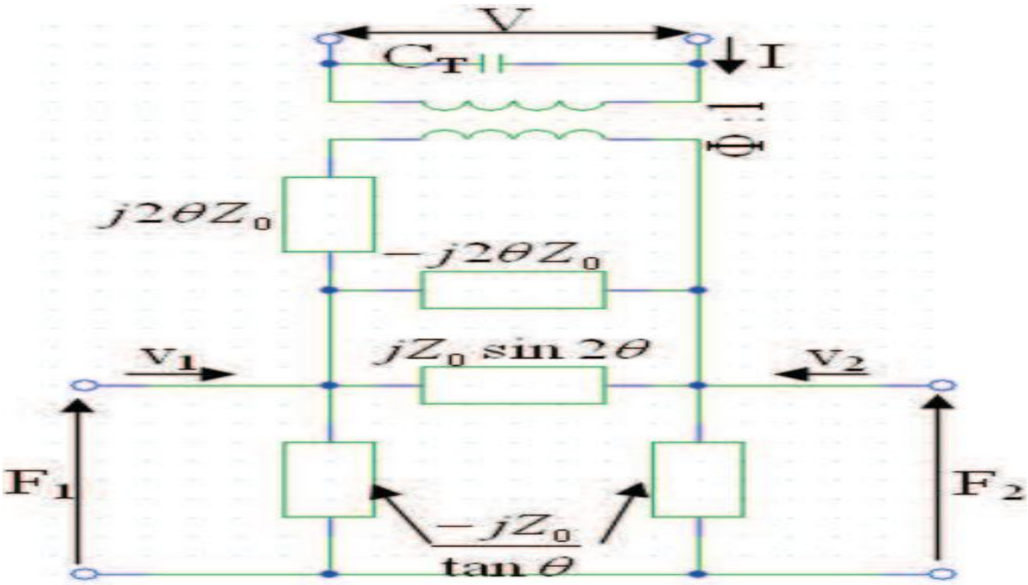

Figure [7]: COM Theory IDT Equivalent Circuit.

The IDT is represented by following Matrix[11]

$$\begin{bmatrix} I \\ v_1 \\ v_2 \end{bmatrix} = \begin{bmatrix} j\omega C_T + \dfrac{\phi^2}{j2\theta Z_0} & \dfrac{\phi}{j2\theta Z_0} & \mp\dfrac{\phi}{j2\theta Z_0} \\ \dfrac{\phi}{j2\theta Z_0} & \dfrac{1}{jZ_0 \tan 2\theta} & \mp\dfrac{1}{jZ_0 \sin 2\theta} \\ \mp\dfrac{\phi}{j2\theta Z_0} & \mp\dfrac{1}{jZ_0 \sin 2\theta} & \dfrac{1}{jZ_0 \tan 2\theta} \end{bmatrix} \begin{bmatrix} V \\ F_1 \\ F_2 \end{bmatrix}$$

Equation 7: COM IDT Matrix.

Where, the matrix parameters equations are shown in the following MATLAB code:

```
%------------------------------------------------------------------
% COM par
Cs=4.6E-10;     % 4.6 pF/Cm for LiNbO3 for testing , actual device uses AlN
Ct=Cs*N;
K11=0;      %coupling coeffiecient form Piezoelectric perturbation
K12=0.0000001;      %coupling coeffiecient form Mechanical perturbation
zeta= 2;     %Constant associated with convention from Electrical to SAW
k=w/vsaw;
ko=(2*pi)/L;
del=k-ko;
B=sqrt(power((del+K11),2)-power(K12,2));
p=(B-del-K11)/K12;
q=1./(del+K11+K12);
Zo=(1-p)/(1+p);
theta=(B*N*L)/2;
phi=2i*N*L*K2;
%---------------------------------------------------------------------
```

Figure [8] : COM IDT EC MATLAB Implementation.

Propagation path based on COM model

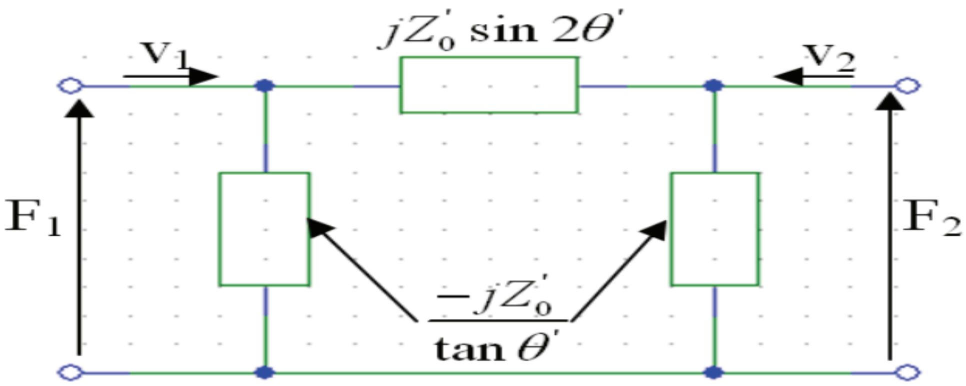

Figure [9] : COM propagation path EC

2.2 Tag Coding Scheme

Surface acoustic wave devices have been widely used in filters presented mobile phones and TVs.[12] The invention of surface acoustic waves RFID has been around for more than 40 years[13] yet it has gained more attention nowadays for numerous reasons such as small tag sizes compared to older models, being completely passive , wide range of operating temeprature and immunity aginst harsh environemnt such as radiation. Moreover SAW RFID tag are simple in design and have wider distance range of operation which puts it on advatage compared conventional RFID tags. [14]

The basic SAW RFID tag structure consists of inter-digital transducer IDT, set of reflectors acting as delay line mounted over a piezoelectric substrate surface. The inter-digital transducer receives interrogating signal from RFID reader/Transceiver via antenna and converts it acoustic wave (much slower than original electromagnetic wave). Each reflector on the substrate surface reflects the acoustic wave back to the IDT after certain delay depends on the reflector position and acoustic wave velocity. [15] The tag identification is encoded by reflector information carried by the reflected signal i.e. delay ,phase , amplitude , orthogonal frequency and/or combination of these information[13] .

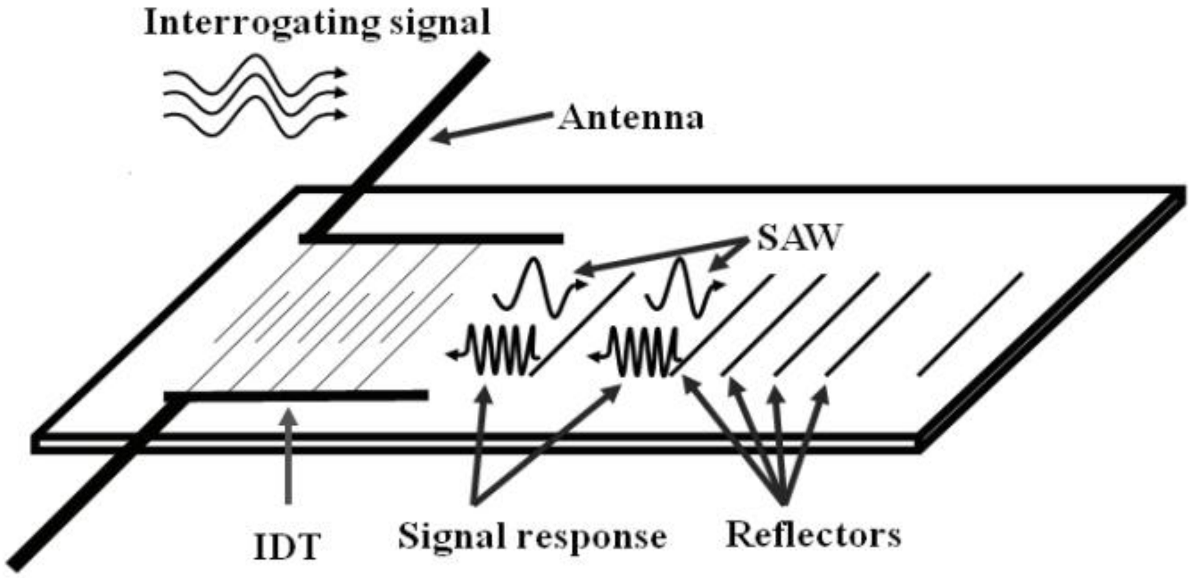

Figure [10]: SAW RFID structure and operation principle

SAW RFID tag code is not stored on memory rather it is implemented physically on the tag surface. Initial delay (chip space between IDT and first reflector) is required for all natural reflections i.e walls and objects to die away.

The widely used technique in commercial SAW RFID is pulse position modulation also known as time position encoding[14] . In this encoding mechanism the delay line is divided into groups of reflector positions termed time slots. Each time slot occupy specific time delay based on the bandwidth $\Delta t = 1/B$, where B is the bandwidth i.e bandwidth of 80 Mhz allows minimum time slot of 12.5 ns.

An example of pulse position encoding is shown in figure 2 where each reflector can be placed in one time slot out of 16 in each group (4-bit encoding per reflector)[16]

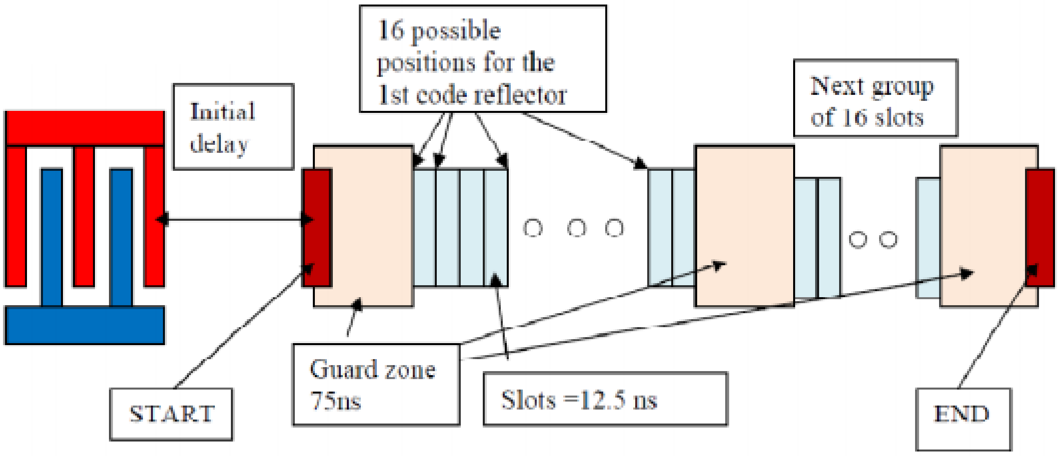

Figure [11]: Example of Pulse position modulation.

A group also can be implemented with 4 time slots (2-bit per reflector) and one or two reflector can be used in one group to maximize the code capacity.[17]

The groups can be placed in single acoustic track as seen in the above figure or in multiple tracks to increase code capacity of the chip , the down side is that the chip size will increase as more than one initial delay space will be required and hence the fabrication cost of the SAW RFID tag.

Other novel approaches to reduce the initial delay space by implementing Z-path delay as shown in figure [3] below to reduce the chip size. Setting the reflecting mirror angle poses as challenge for this approach.[18]

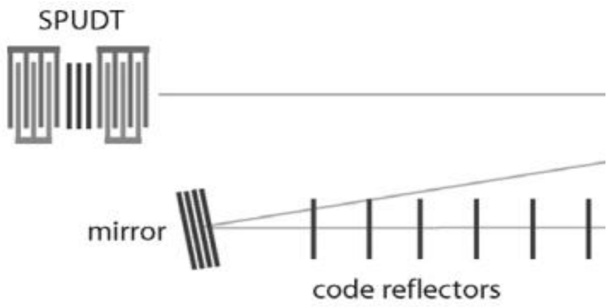

Figure [12]: Z-path tag geometry

Using pulse position encoding technique simplifies the reader decoding algorithm and consequently reader design. On the other hand the narrower the time slot width the more resolution to read time difference between symbols required from the reader .[14]

According to Ken-ya Hashimoto (2005-2006) pulse position modulation tags carry the advantage of low sensitivity to small temperature and velocity variations and has small insertion loss.

Another SAW RFID tag ID coding technique is phase encoding. This method utilizes the phase

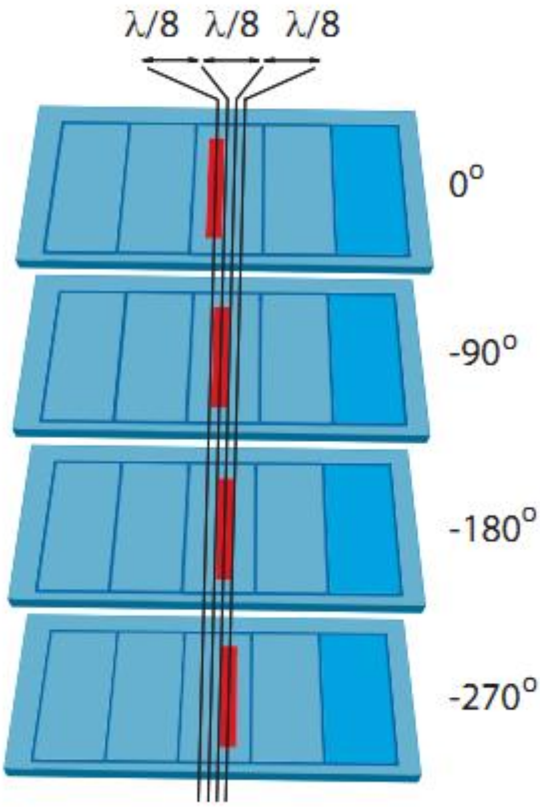

Figure [13] : Phase Encoding

shift information of the reflected signal. The phase shift of the reflected signal is related to the position of the reflector[14]. For example a reflector can encode 2-bit information by shifting the reflector position by λ/8 , which contribute to phase shift of 90 degrees , as shown in figure 4.[17]

Phase encoding allows for high code capacity of SAW RFID tag specially when combined with other method like pulse position modulation.

When designing SAW RFID tag with phase information encoding the temperature effect on phase information should be cancelled with cautious as it may cause error in reader phase interpretation also surface acoustic wave velocity variation can affect the reflected encoded phase values.[19]

Orthogonal Frequency coding method is also used to code the tag information with low loss reflectors (50%-75%) compared to CDMA tags[20] The OFC reflectors for certain frequency is called chip and when designed in proper manner is completely transparent to other chips and is orthogonal in both frequency and time as seen in figure 5.

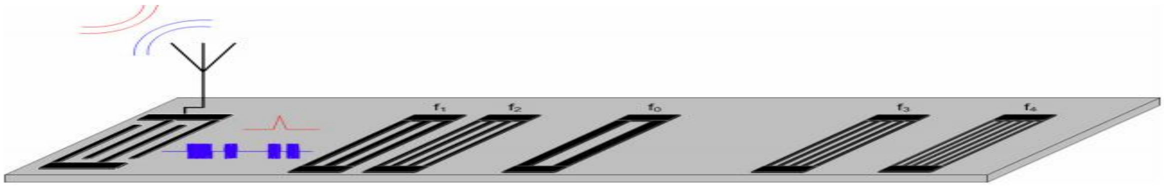

Figure [14]: OFC Encoding

The code is then built by using random chips in sequence, also using phase or pulse position modulation can significantly increase the code capacity [21] as shown in figure 6 below

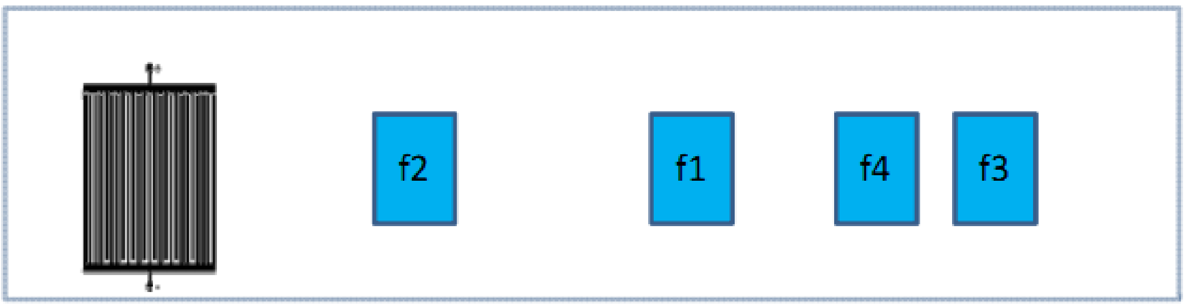

Figure [15]: Schematic of an OFC TDM embodiment

The major advantage of OFC is the low loss, hence wider operation range but it is hard to achieve a resonator with high Q-factor[14].

In addition to previous methods, amplitude modulation can also be used where reflector presence is interpreted by reader as ON(1) ,the absence of reflected amplitude (OFF reflector structure with same damping but not reflective as ON structure is used to achieve uniformity) is interpreted as OFF(0) .this method produces high insertion loss and thus shorter range.

2.3 Piezoelectric material of choice

Device to be implemented on Aluminum nitride for several reasons such as :

- Good Dielectric properties
- Close to that of Silicon Non-reactive with normal semiconductor process chemicals and gases
- Low fabrication cost especially at high frequency SAW operation due to high acoustic velocity.

Aluminum Nitride (AlN) also shows higher SAW wave velocity thus allowing lower fabrication cost for higher frequency SAW tags. [5]

$$KhAlN = 2 * \pi * \frac{h}{\lambda}$$ where h is AlN layer thickness

Equation 8:Normalized thickness

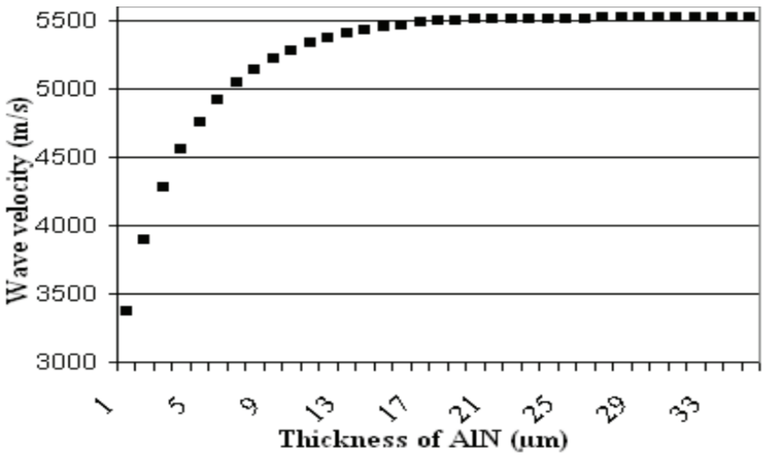

Wave velocity in structure AlN/SiO_2(1.3μm)/Si(4μm) with different thicknesses of AlN

Figure [16]: SAW velocity Vs. AlN Thickness

The saw velocity reaches around 5500 m/s compared to 3997 m/s for LiNbO3. AlN also exhibit good dielectric properties ε=8.5 and high thermal conductivity Low thermal expansion coefficient.

In study done by [5] AlN have high coupling coefficient compared to Quartz and other piezoelectric materials.

The electromechanical coupling factor k describes the efficiency of the transduction of the piezoelectric material between mechanical and electrical energy and vice-versa:

$$K = \sqrt{\frac{Mechanical\ energy\ stored}{Electrical\ energy\ applied}}$$

$$K = \sqrt{\frac{Electrical\ energy\ stored}{Mechanical\ energy\ applied}}$$

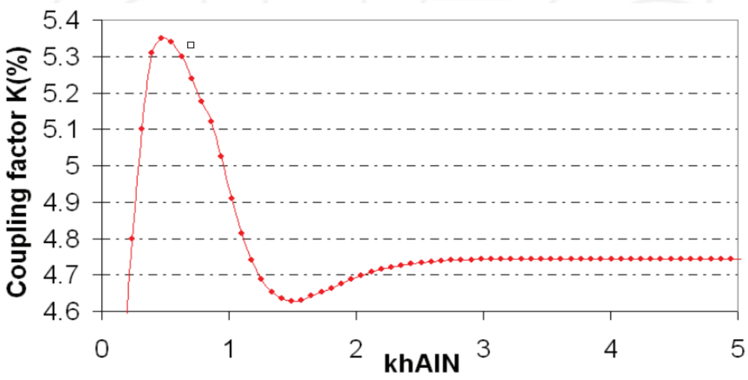

Calculated values of coupling factor K(%) in SAW device AlN/Si substrate depends on the normalized thickness khAlN of AlN layer

Figure [17] : Coupling Coefficient Vs AlN thickness.

The electromechanical coupling factor is often expressed in terms of K^2, which is the percentage of energy retained after transduction. To maximize device efficiency, a material with a high electromechanical coupling factor should be chosen.[4]

To summarize, Simulation and modeling of IDT is crucial to define device parameters such as, centre frequency, number of finger pairs, finger width, finger spacing and aperture, and frequency response of the system.

Two Equivalent Circuit Models were studied; Mason's EMC, COM model, to understand on physical behavior of the device.

SAW RFID coding uses different methods based on information of reflected signal such as delay, phase, amplitude and orthogonal frequency. Sometimes combination of more than one encoding techniques is used to increase coding capacity. Pulse position modulation is less sensitive to velocity and temperature variation, as well as simple implantation for both tag and reader system. The code capacity can reach $18 * 10^{18}$ unique IDs. The major objectives of SAW tag design include a reduction of device losses to maximize the range, a reduction of device size to save manufacturing and fabrication cost, and an enhancement of data capacity to allow higher code density and more unique IDs.

Aluminum nitride (AlN) is chosen as piezoelectric material due to its high SAW velocity speed, higher coupling factor, cheaper fabrication cost and its chemical characteristics close to that of Silicon Non-reactive with normal semiconductor process chemicals and gases

CHAPTER 3

METHODOLOGY/PROJECT WORK

3.1 Tag Schematic

- Design of 2-bit coding tag (3 reflectors)

  The first reflector is reference at 1us delay, the first reflector is 0.1 us from Reference reflector representing code 0 , while delay of 0.15 us represents code of 1.
  Having 2 reflectors allows 8 possible combinations

- Implanted on Lithium Niobate (SAW velocity = 3997 m/s)

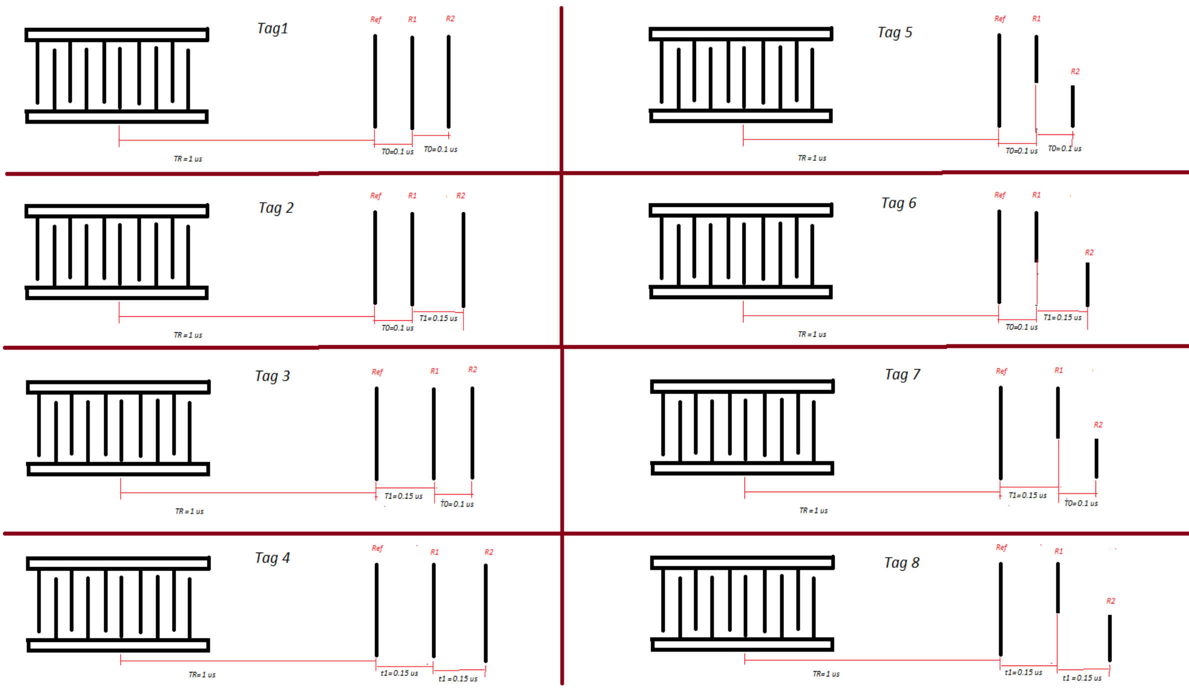

Figure [18]: Tag layout.

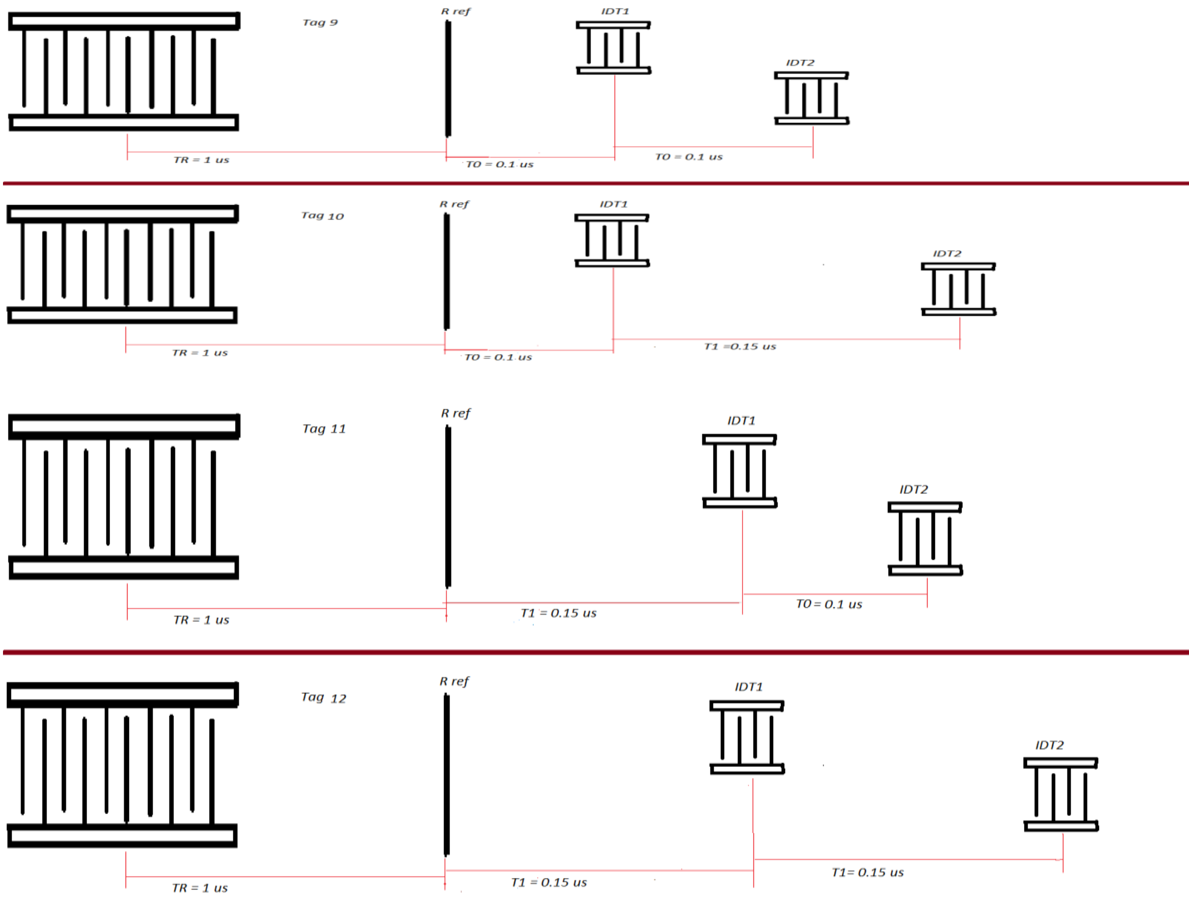

Figure [19] :Tag layout using IDT as reflectors.

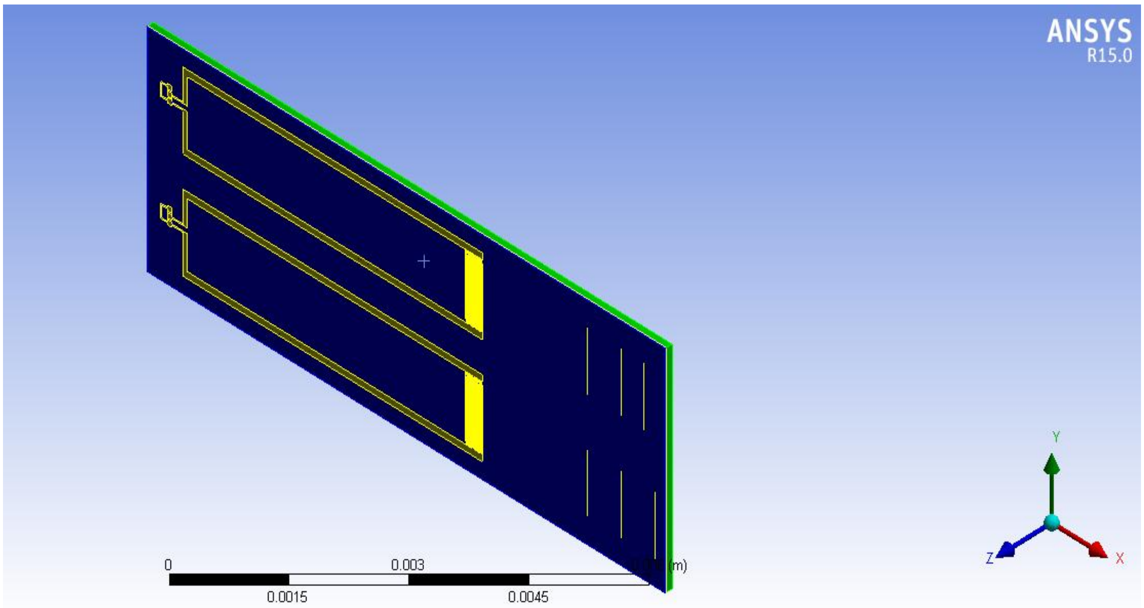

Figure [20] :Tag 3D Rendering using ANSYS 15

3.2 Device Equivalent Circuit Model

A) Equivalent circuit model based on mason's model is constructed using MATLAB for:
   1- IDT
   2- Propagation path.
   3- SAW delay line (input IDT-propagation path-output IDT)
   4- SAW tag 1 (input ID- propagation path- reflector)[22]
   5- SAW tag 2 (input ID- propagation path 1- reflector1- propagation path 2- reflector 2)[22]

B) Equivalent Circuit parameters calculated based on COM theory for IDT and Propagation path.

Complete MATLAB Codes are Provided in Appendices I

For Mason's ECM, admittance parameter is calculated for the 3 port network (2 acoustic, 1 electrical) and transformed to S-parameters.

For further simplify the circuit and enable cascading of propagation path and other device elements, the admittance parameters are converted to ABCD parameters with one port connected to G0.

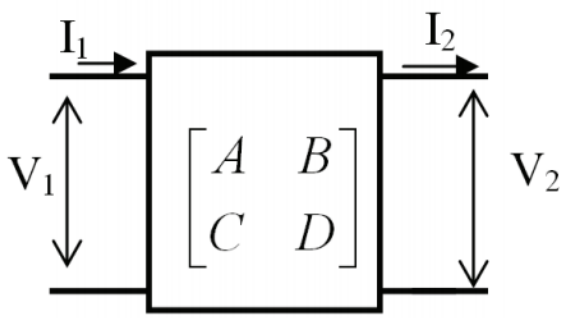

Figure [21]: ABCD representation of two ports IDT.

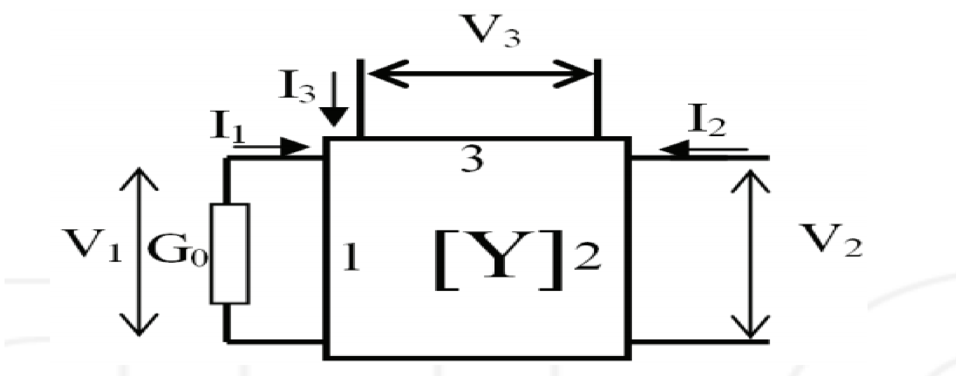

Figure [22]: Two port network of IDT.

```
%-------------------------------------------------------------------------
%-------------------------------------------------------------------------
% ABCD Matrix for IDT
x=Np*pi*((f-fo)/fo);
A=((2.*x)-1i)./(1i*4*Np);
B=(1./Go).*(A);
C=(pi.*f*Cs.*x)-(4*Np.*Go)-1i*((0.5*pi.*f*Cs)+((4*Np.*Go)./((2.*x)-1i)))
D=(pi*f*Cs*Ro.*x)-(4*Np)-(1i*0.5*pi*f*Cs*Ro);
Ain=A;
Bin=B;
Cin=C;
Din=D;
Aout=Din;
Bout=Bin;
Cout=Cin;
Dout=Ain;
check=(A.*D)-(B.*C);        % check   is equal to 1
%-------------------------------------------------------------------------
```

Figure [23]: IDT ABCD cascade Matrix.

ABCD parameters simplifies cascade configuration of the device as

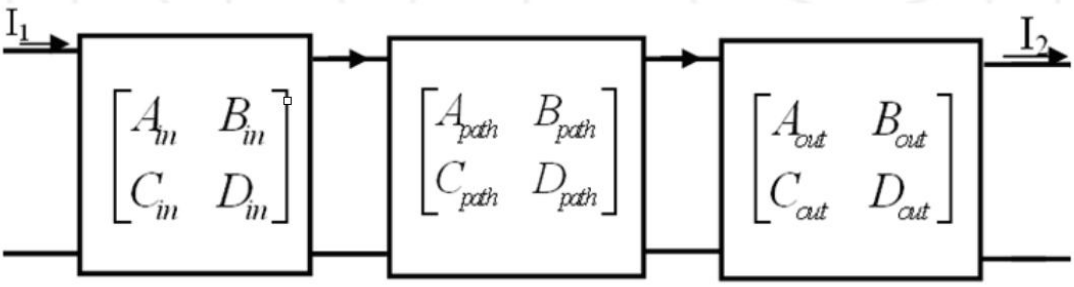

Figure [24]: Cascade ABCD matrix of input IDT propagation path output IDT

For reflectors, it can be considered as single pair IDT with no electric port, and is modeled that way based on mason's ECM.

Coupling of mode Equivalent model is implemented by calculating the schematic impedance values so that it can be used in spice simulation using Advanced System Design Software.

```
%----------------------------------------
% circuit schematic paramters
%IDT
imped1=2i*theta.*Zo;
imped2=1i*Zo.*sin(2*theta);
imped3=(-1i.*Zo)./tan(theta);
%propagation path
imped4=1i*conj(Zo).*sin(2*conj(theta));
imped5=(-1i*conj(Zo))./tan(conj(theta));
```

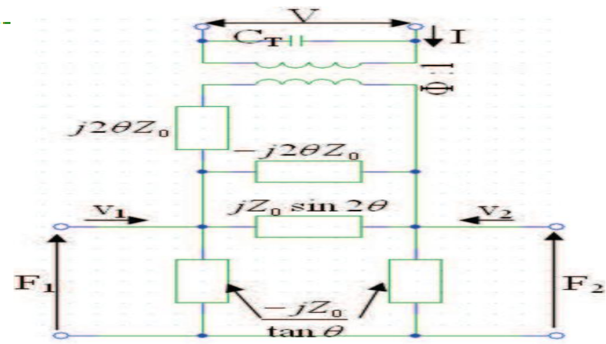

Figure [25] : COM EC implementation in MATLAB.

3.3 Aluminum Nitride Delay line characterization

3.3.1 Objectives

To extract:

1- Center frequency
2- SAW velocity
3- Coupling coefficient

3.3.2 Methodology

The provided scattering parameters can’t be used o extract the resonant frequency directly without processing to smooth and remove all unwanted signals.

To extract Center frequency information, S21 and S12 parameters are analyzed using Matlab to remove unwanted signals such as:

1- Feed through effect of the input IDT on output IDT.
2- Unwanted reflections of higher orders.

This is achieved by converting the frequency response of the device into time domain first and applying time gating to the wanted signals and discarding the rest of the response then reconverting the signal into frequency domain to have a clear view of the center resonant frequency.

Time gating is applied at time zero to remove the feed through effect by the use of rectangle window and at 1microsecond to capture first reflection using Blackman window.

Based on centre frequency information SAW velocity can be calculated as follow

$$v_{SAW} = \lambda * f_{o\ (measured)}$$

Where f_o is resonant frequency of IDT

CHAPTER 4
RESULTS AND DISCUSSION

4.1 Simulation

Based on Mason's ECM, the following graphs represents the admittance and scattering S parameters

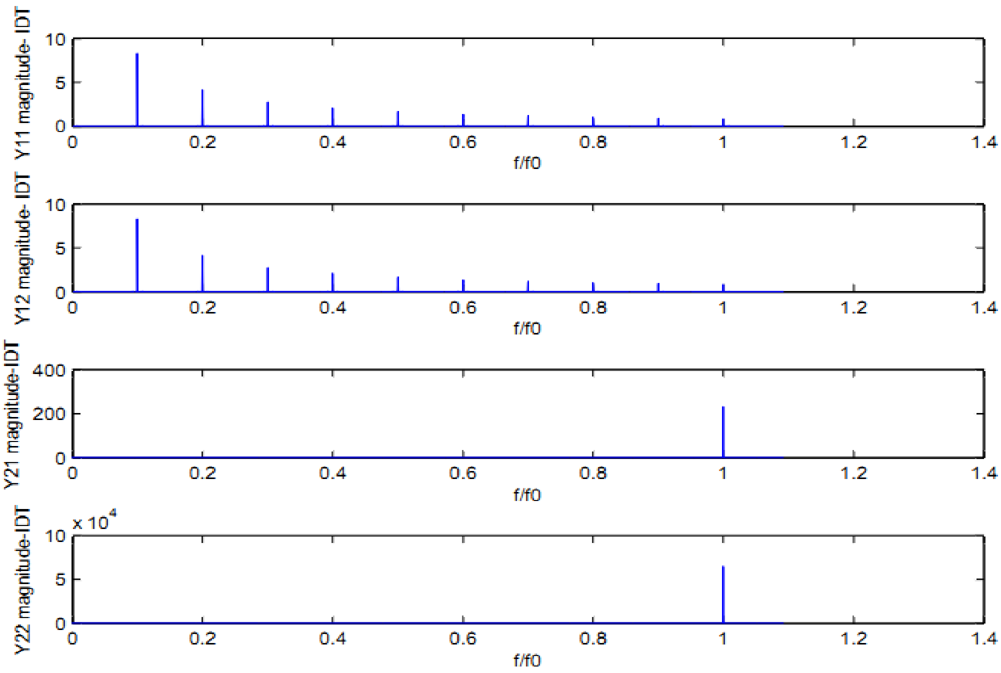

Figure [26] :IDT Admittance.

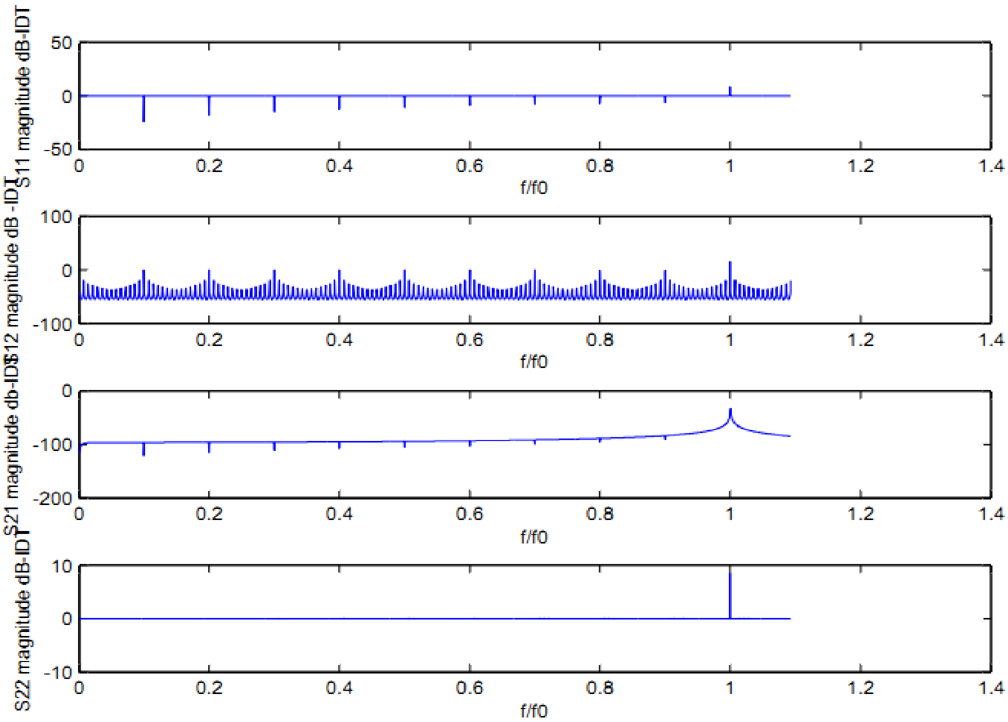

Figure [27] : IDT Scattering Parameters.

S_{11}, the *return loss*, is a measure of the power returned to the source. When there is no reflection from the load, or the line length is zero, S_{11} is equal to the reflection coefficientS_{21}, the insertion loss, is a measure of the power transmitted from port 1 to port 2

As seen the insertion loss of IDT is minimum at central frequency of with insertion loss -34.43 dB.

For delay line simulation the insertion loss of the device is -0.7928 dB

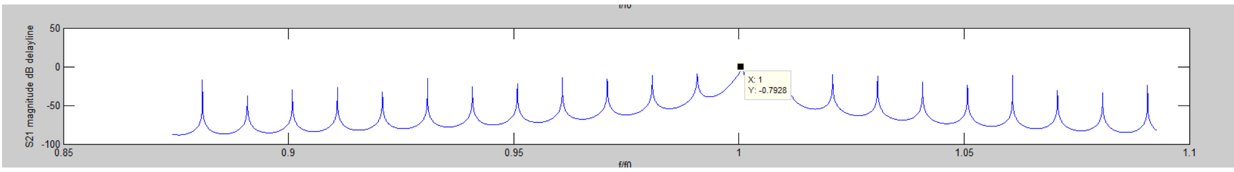

Figure [28]:Delay line insertion loss.

Scattering parameters for the following circuit configuration is Appendices

1- Simple delay line (input IDT-propagation path-output IDT) Appendix III
2- Simple tag (input ID- propagation path- reflector) Appendix IV
3- Simple tag (input ID- propagation path 1- reflector1- propagation path 2- reflector 2)
   Appendix V

COM theory impedance calculation (real and imaginary) is presented in Appendix VI

For the Tag circuit based on mason’s ECM model on Matlab , the model requires adding interrogation signal , the mathematics implementation of which is still under study.

4.2 Results and Discussion (ALN Delay lines)

4.2.1 Background

The received frequency response covered 7 Delay lines fabricated on ALN with following specs.

Table 1: AlN Delay lines specifications.

Device Name	Finger width (W_f) µm	Finger Spacing (S_f) µm	Acoustic Wavelength (λ) µm	Bus Bar Height BBH (µm)	Central Frequency (MHz)	Acoustic Aperture (*Ha*) µm	Finger Length (L_f)	No. of Fingers (*N*)	Delay (*D*) µm
B1	2	2	8	40	700	264.96	291.44	72	5600
C1	3	3	12	60	466.66	397.43	437.16	72	5600
A2	1	1	4	20	1400	132.48	145.72	28	5600
B2	2	2	8	40	700	264.96	291.44	28	5600
A3	1	1	4	20	1400	132.48	145.72	72	5600
B3	2	2	8	40	700	264.96	291.44	28	5600
G1	1.5	1.5	6		934			72	5600

4.2.2 Extracting centre Frequency of Delay line:

Device B1, the original VNA measurements is shown in the figure below:

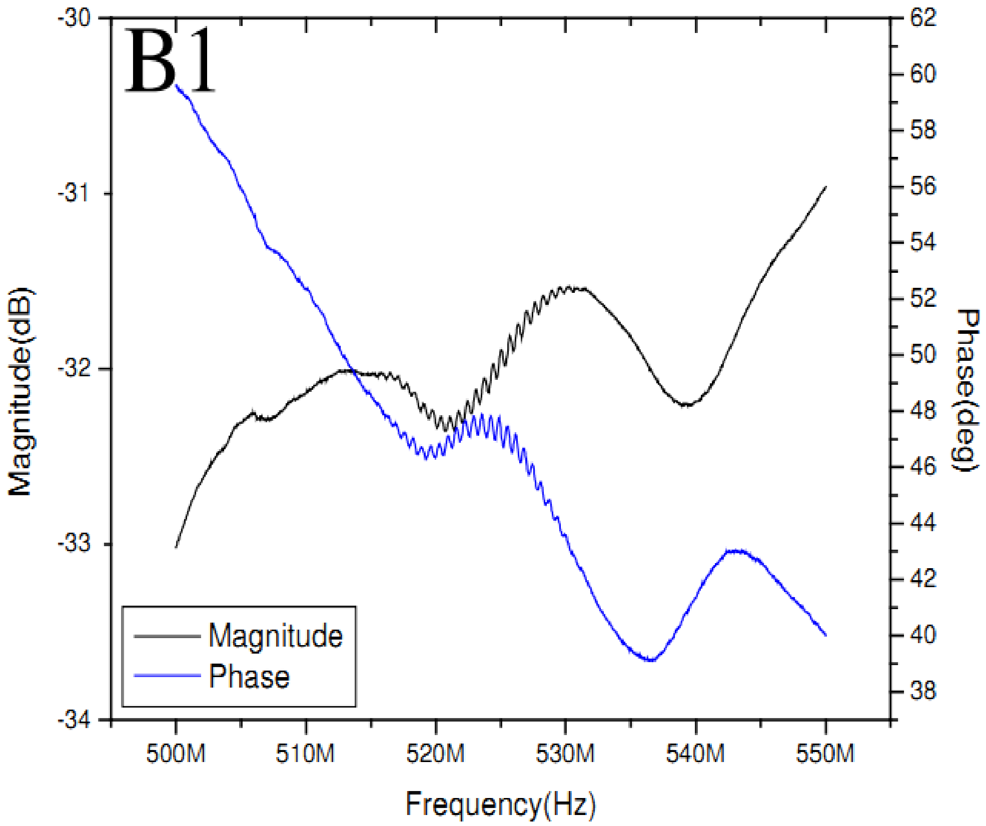

Figure [29]: Device B1 insertion loss before processing.

The plot is not clear on centre frequency response and cannot be compared to simulation results. Thus data processing is needed.

The next figure shows the exact same scattering parameter (S21) after being processed. The impulse response information reflects the position of the signals that needs to be removed. We are interested in the first order reflection of the output IDT. This time gating is applied as seen to capture it. Also the whole response without the feed through is captured.

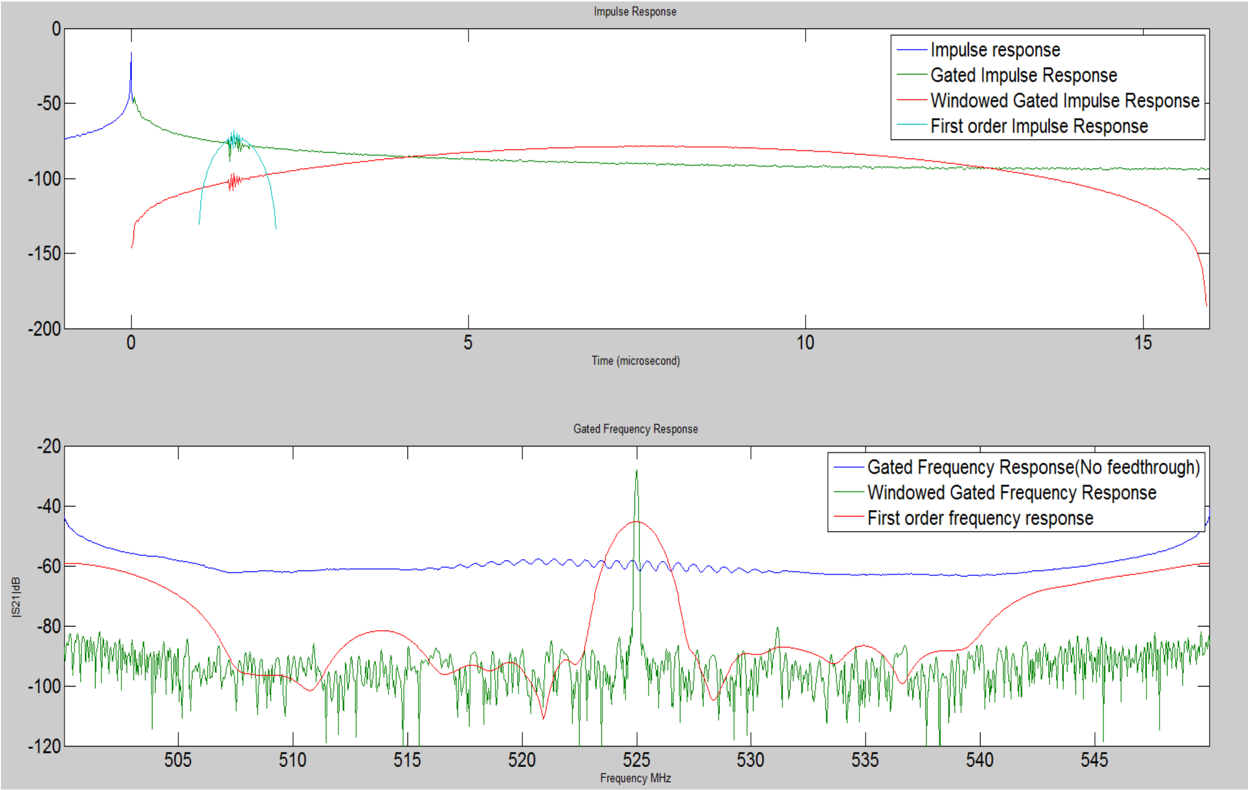

Figure [30] : Device B1 impulse and Frequency response after processing.

As seen from the figure above after processing the signal in time domain we convert back to frequency domain. From the plot it is quite clear that the center frequency is 525 MHz.

The same procedures are applied to the rest of the devices for both S11 and S21 parameters. The complete results are tabulated below.

Table 2 : Delay lines design and measured center frequencies

Device Name	Central Frequency (MHz)	Measured Frequency (MHz)
B1	700	525
C1	466.66	380
A2	1400	952
B2	700	525
A3	1400	950
B3	700	525
G1	934	660

4.2.3 *SAW velocity extraction:*

For SAW velocity extraction, by knowing the center frequency and design wavelength we can calculate the velocity with simple equation

$$v_{SAW} = \lambda * f_{o\,(measured)}$$

where f_o is resonant frequency of IDT

Equation 9 : SAW velocity calculation.

The results are tabulated for all devices:

Table 3: AlN Delay lines Measured SAW velocities.

Device Name	Acoustic Wavelength (λ) µm	Measured Frequency (MHz)	Measured Velocity (m/s)
B1	8	525	4200
C1	12	380	4560
A2	4	952	3700
B2	8	525	4200
A3	4	950	3800
B3	8	525	4200
G1	6	660	3960

The expected SAW velocity of the devices is calculated by constructing a model based on each layer thickness.

The energy is confined within the depth of 10 wavelengths in the device with 90% of the energy in the first wavelength depth.

Thus if the piezoelectric layer is thin the SAW velocity is dependent of that of silicon substrate. Two mathematical models were built. The first is based on SAW velocity in each layer and the density of each material. The other model is based on the confined energy percentages in each layer

4.2.3.1 First Model Results:

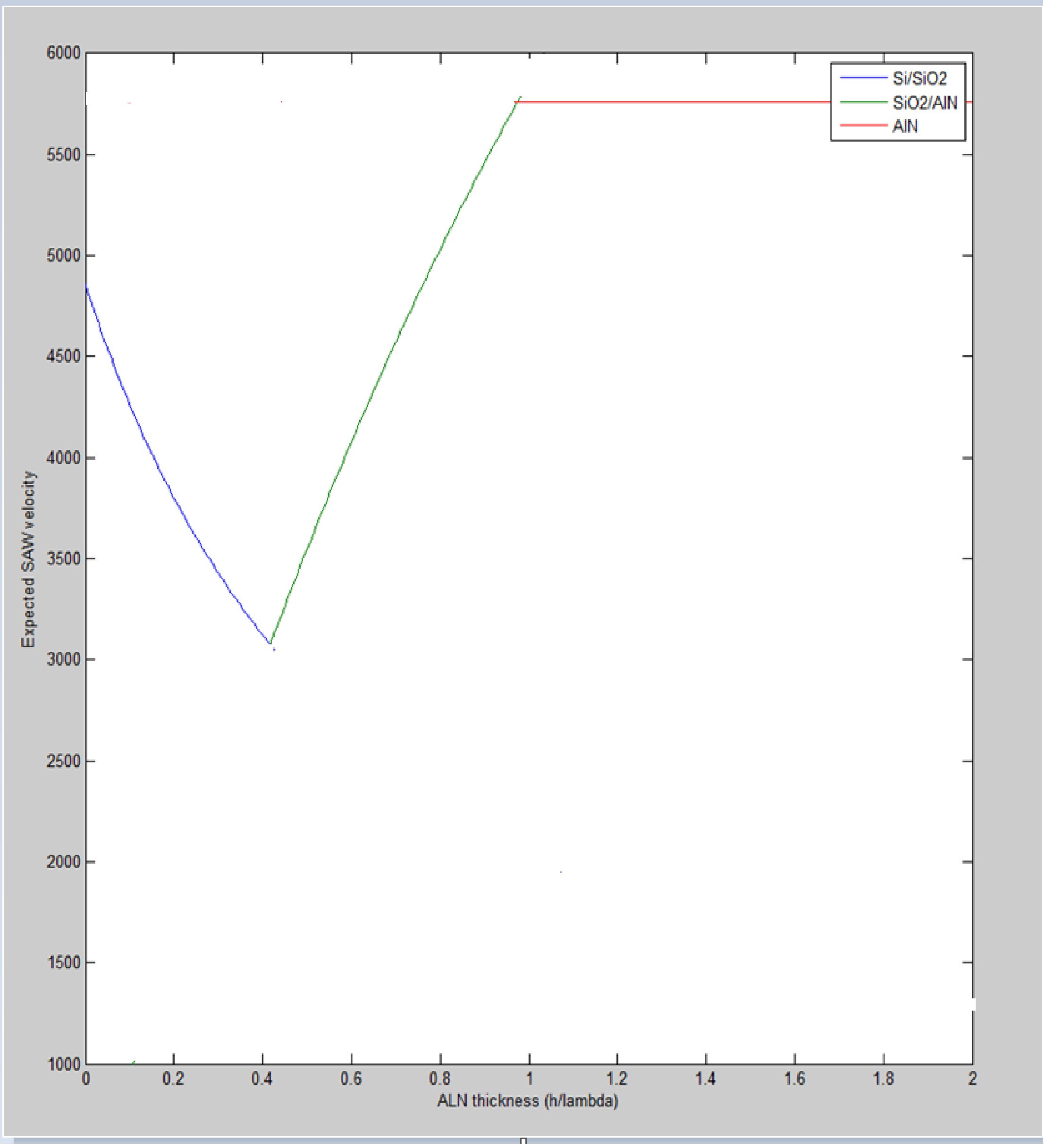

Figure [31]: SAW velocity versus normalized AlN thickness.

For thin Aluminum nitride films the SAW velocity is dependent on that of silicon as seen in first section of figure.

At normalized length of 1 (AlN is equal to 1 wavelength) the SAW velocity is closely equal to 5700 m/s which is the Rayleigh velocity of Aluminum nitride.

Table 4 : Expected and measured SAW velocity.

Device Name	Measured Velocity (m/s)	Expected SAW velocity	Error %
C1	4560	4317	5.628909
B1	4200	4090	2.689487
B2	4200	4090	2.689487
B3	4200	4090	2.689487
G1	3960	3918	1.071975
A2	3700	3532	4.756512
A3	3800	3532	7.587769

4.2.3.2 Second Model Results:

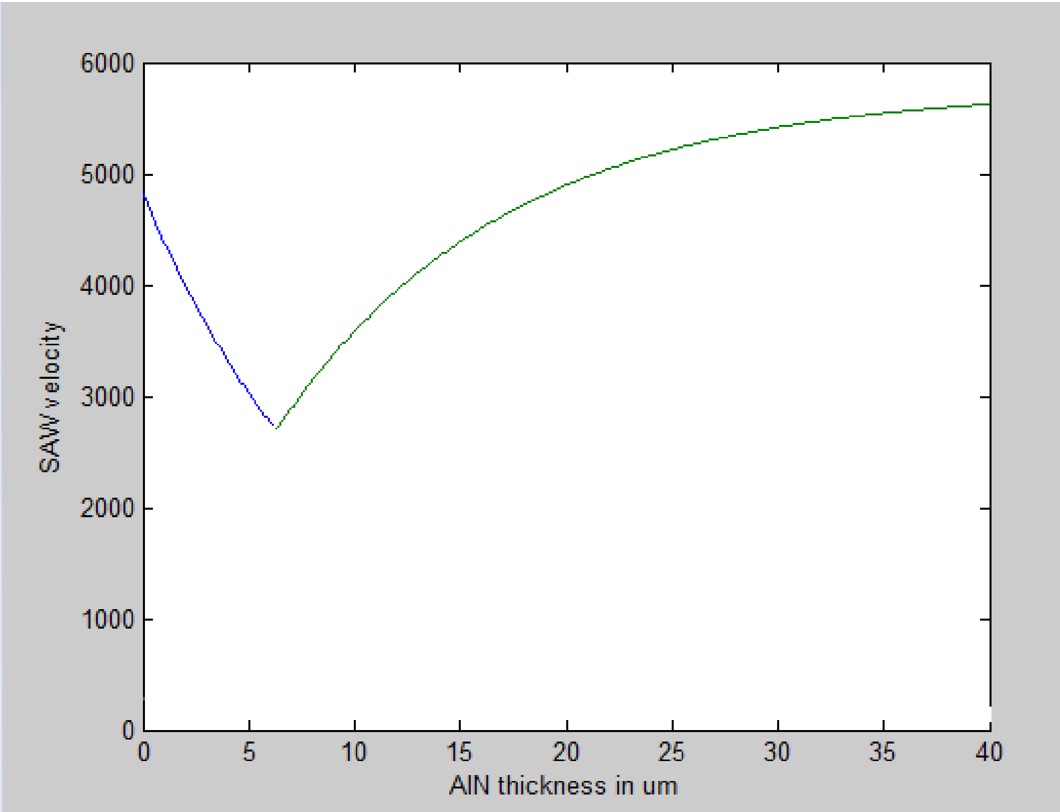

Figure [32]: Expected SAW Vs. AlN thickness.

Table 5: Expected SAW velocity based on model 2.

Device Name	Measured Velocity (m/s)	Refined model	Error %
C1	4560	4441	2.679577
B1	4200	4229	-0.68574
B2	4200	4229	-0.68574
B3	4200	4229	-0.68574
G1	3960	4028	-1.68818
A2	3700	3656	1.203501
A3	3800	3656	3.938731

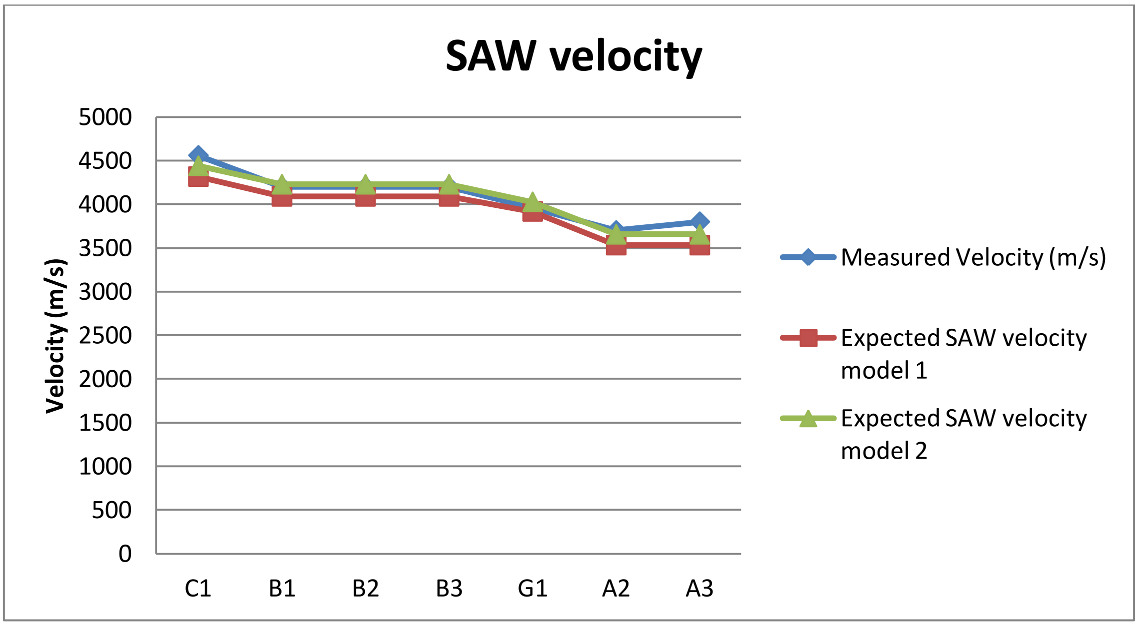

Figure [33] : Measured Vs. Expected Saw Velocity.

It is clear from figure [32] above that the measured velocity is very close to the expected one with minimum error percentage of 0.68 % and maximum error of 3.9 % (model 2)

It is also evident that model 2 is more accurate than model 1 as it is based on energy distribution in each layer rather than material density.

4.2.4 Coupling Coefficient (K^2):

Admittance information is used to calculate the coupling Coefficient[23]

$$k^2 = \frac{1}{8N^2 f_c} \cdot \frac{G_0}{C_s}$$

$$k^2 = \frac{\pi}{4N} \cdot \frac{G_0}{B_0}$$

Where N is a number of IDT electrode finger pair, and fc is the center frequency. G_0, C_s, and B_0 are the radiation conductance, capacitance and susceptance of center frequency response, respectively

Equation 10 : Coupling Coefficient calculation.

The radiation conductance and be extracted directly from admittance parameters as[24]:

$$Y_{11} = Y_{22} = G_a + j(B_a + \omega \cdot C_t)$$

Equation 11:Radiation conductance calculation

At centre frequency :

$$Y_{11} = G_0 + j(B_0 + 2\pi f_o C_T)\ ,where\ C_T = N_p * H_p * C_s$$

Where Np is number of electrode pairs, Ha is aperture and Cs is capacitance per unit length.

Bu et al (2004) [25] reported that Cs for ALN is about 79 pF/m. based on these information coupling coefficient is calculated and tabulated as bellow

Table 6: Coupling Coefficient of AlN Delay lines

Device Name	$K^2\%$
B1	0.117
C1	0.102
A2	0.136
B2	0.126
A3	0.128
B3	0.116
G1	0.139

The results corresponds to what [26] has reported as part of literature . ($K^2\%\ from\ 0.15 - 0.8$)

CHAPTER 5
CONCLUSION

SAW RFID coding uses different methods based on information of reflected signal such as delay, phase, amplitude and orthogonal frequency. Sometimes combination of more than one encoding techniques is used to increase coding capacity. Pulse position modulation is less sensitive to velocity and temperature variation, as well as simple implantation for both tag and reader system. The code capacity can reach $18 * 10^{18}$ unique IDs.

To successfully implement the device, proper modeling and simulation is carried out to extract device physical and response parameters such as centre frequency, finger pairs' number, spacing, scattering parameters and frequency response of the system. The equivalent circuit model is used in this study due to faster simulation speed and efficiency. Using MATLAB , the device is modeled using Mason's ECM and COM theory model.

Important device characteristics such as center frequency, SAW velocity and coupling coefficient need to be measured to determine device characteristics and compare it to simulated results.

In order to do that, impulse response data is obtained from scattering parameters and time gating is applied to remove unwanted reflections and feed through effect then converted back to frequency response for clearer view of data.

Saw velocities depend on center frequency and the device as device deviates from its designed frequency, the velocity is affected and thus the time delay. Two models were built to investigate expected SAW velocities. The error range between measure and expected is between [0.68 -3.9 %].

Coupling coefficient is obtained with help of processing admittance Y_{11} of the device. The results obtained showed $K^2\% = 0.102 - 0.139$.

In order to have higher reflected energy (amplitude) of output IDT proper matching should be done to both IDTs. Matching network is under investigation and results should be showed in following report.

The tags sent for fabrication have not arrived so far from fabrication house. Characterization and measurements will be carried out once devices are available.

REFERENCES

[1] A. S. a. T. Nomura, "Wireless sensor system using surface acoustic wave devices," *CCAS-SICE*, pp. 2359-2363, 2009.

[2] D. P. Morgan, "Surface Acoustic Wave Devices," in *Encyclopedia of RF and Microwave Engineering*, ed: John Wiley & Sons, Inc., 2005.

[3] G. G. V. Kutiš*a, V. Královiþa, I. Rýgerb, E. Mojtoa, T. Lalinský, "Modelling and simulation of SAW sensor using FEM " *Procedia Engineering*, vol. 48, pp. 332-337, 2012.

[4] J. Kirschner, "Surface Acoustic Wave Sensors (SAWS):Design for Application," *MICROELECTROMECHANICAL SYSTEMS*, DECEMBER 6, 2010.

[5] T. Hoang, "SAW Parameters Analysis and Equivalent Circuit of SAW Device " in *Acoustic Waves - From Microdevices to Helioseismology*, P. M. G. Beghi, Ed., ed: InTech, 2011.

[6] S. Hartmann, "A global SAW ID tag with large data capacity," *Ultrasonics Symposium Proceedings. 2002 IEEE*, vol. 1, pp. 65-69.

[7] K.Nakamura, "A Simple Equivalent Circuit For Interdigital Transducers Based On The Couple-Mode Approach," *IEEE Transactions on Ultrasonics, Ferroelectrics, and Frequency Control*, vol. 40, pp. pp.763-767, November 1993 1993.

[8] K.-Y. Hashimoto, *Surface Acoustic Wave Devices in Telecommunications Modelling and Simulation*, 2000.

[9] A. B. B. S. T. a. S. Majumdar, "SPICE Simulation of Surface Acoust Wave Interdigital Transducers," *IEEE TRANSACTIONS ON ULTRASONICS, FERROELECTRICS, AND FREQUENCY CONTROL*, vol. 42, pp. 784-786, 4, JULY 1995 1995.

[10] W. C. Wilson and G. M. Atkinson, "Rapid SAW Sensor Development Tools," 2007.

[11] K. Nakamura and K. Hirota, "Equivalent circuits for unidirectional SAW-IDTs based on the coupling-of-modes theory," *Ultrasonics, Ferroelectrics and Frequency Control, IEEE Transactions on*, vol. 43, pp. 467-472, 1996.

[12] A. Saitoh and T. Nomura, "Wireless sensor system using surface acoustic wave devices," in *ICCAS-SICE, 2009*, 2009, pp. 2359-2363.

[13] C. S. Hartmann, "A global SAW ID tag with large data capacity," in *Ultrasonics Symposium, 2002. Proceedings. 2002 IEEE*, 2002, pp. 65-69 vol.1.

[14] V. P. Plessky and L. M. Reindl, "Review on SAW RFID tags," *Ultrasonics, Ferroelectrics and Frequency Control, IEEE Transactions on*, vol. 57, pp. 654-668, 2010.

[15] X. Xia and C. Zhigang, "Finite element analysis of harmonic frequency for 2.4GHz SAW tags," in *Electron Devices and Solid-State Circuits (EDSSC), 2011 International Conference of*, 2011, pp. 1-2.

[16] V. Plessky, T. Ostertag, V. Kalinin, and B. Lyulin, "SAW-tag system with an increased reading range," in *Ultrasonics Symposium (IUS), 2010 IEEE*, 2010, pp. 531-534.

[17] S. Harma, W. G. Arthur, R. G. Maev, C. S. Hartmann, and V. P. Plessky, "P0-14 Inline SAW RFID Tag Using Time Position and Phase Encoding," in *Ultrasonics Symposium, 2007. IEEE*, 2007, pp. 1239-1242.

[18] S. Harma, V. P. Plessky, C. S. Hartmann, and W. Steichen, "Z-path SAW RFID tag," *Ultrasonics, Ferroelectrics and Frequency Control, IEEE Transactions on,* vol. 55, pp. 208-213, 2008.

[19] K.-y. Hashimoto, *2005-2006 International ,Distinguished Lecturer Program,* 2005-2006.

[20] D. C. Malocha, J. Pavlina, D. Gallagher, N. Kozlovski, B. Fisher, N. Saldanha, *et al.*, "Orthogonal frequency coded SAW sensors and RFID design principles," in *Frequency Control Symposium, 2008 IEEE International*, 2008, pp. 278-283.

[21] D. Malocha, N. Kozlovski, B. Santos, J. Pavlina, M. A. Belkerdid, and T. J. Mears, "Ultra wide band surface acoustic wave (SAW) RF ID tag and sensor," in *Military Communications Conference, 2009. MILCOM 2009. IEEE*, 2009, pp. 1-7.

[22] A. H. R. F. D. A. O. Dahmane, "A New SAW Device Simulator Based on Mason's Equivalent Circuit Model," presented at the The Fourth International Conference on Sensor Device Technologies and Applications, 2013.

[23] M.-J. P. Cheol-Yeong Jang, Eun-Ja Jung, Hyun-Chul Choi, Jung-Hee Lee and Yong-Hyun Lee, "Device Characteristics of Radio Frequency SAW Filter Fabricated on GaN Thin Film," *Journal of the Korean Physical Society,* vol. 42, pp. S482-S482, February 2003.

[24] L. V. M. Clement , J. Sangrador, E. Iborra, A. Sanz-Hervas, "SAW characteristics of AlN films sputtered on silicon substrates," *Ultrasonics* vol. 42, pp. 403-407, 2004.

[25] D. C. G. Bu, M. Shur,L. J. Schowalter S. Schujman,R. Gaska, "Electromechanical coupling coefficient for surface acoustic waves in single-crystal bulk aluminum nitride," *APPLIED PHYSICS LETTERS,* vol. 84, 7 June 2004.

[26] M.-J. P. Sun-Ki Kim, Cheol-Yeong Jang, Hyun-Chul Choi, Jung-Hee Lee, and Yong-Hyun Lee, "Characteristics Analysis of Saw Filter Using Al 0.36Gao.6 4 N Thin Film," in *Materials Research Society Symposium Proceedings*, San Francisco, California, 2002, pp. 51-56.

APPENDICES

A. Appendix I: Mason's ECM Matlab code


```
%---------------------------------
% Device Specification
f=0:500000:1000000000;
BW=26;
fo=915000000;
pi=3.1416;
Rin=50;
%---------------------------------
% Material properties
vsaw=3978;      % need to change for ALN
wavlength=vsaw/fo;
%---------------------------------
% IDT Specs.
width=wavlength/4;
spacing=width;
Np=70;
l=50*wavlength;      %propagation path length
%---------------------------------
% Material properties
K2=4.5/100;
Cs=4.6E-10;      % 4.6 pF/Cm for LiNbO3
Ha=(1/Rin)*(1/(2*fo*Cs*Np))*((4*K2*Np)/((4*K2*Np*4*K2*Np)+(pi*pi)));
%-----------------------------------
% Mason's ECM for IDT
alpha=(pi*f)/(2*fo);
Ro=(1)/(fo*Cs*K2*K2);
Go=(1/Ro);
%-----------------------------------
% Y paramters calculation
Y11=-1i*Go*cot(4*Np*alpha);
Y12=(1i*Go)./(sin(4*Np*alpha));
Y13=-1i*Go*tan(alpha);
Y33=1i*Np*((2*pi*f*Cs)+(4*Go.*tan(alpha)));
%------------------------------------
Y22=Y11;
Y21=Y12;
Y31=Y13;
Y23=-Y13;
Y32=-Y13;
Y=[Y11 Y12 Y13;Y21 Y22 Y23;Y31 Y32 Y33];
%-----------------------------------------
%Y paramters plotting vs. frequency
figure(1);
subplot(411)
plot(f/fo,abs(Y11));
xlabel('f/f0');
ylabel('Y11 magnitude- IDT')
subplot(412)
plot(f/fo,abs(Y12));
xlabel('f/f0');
ylabel('Y12 magnitude- IDT')
subplot(413);
plot(f/fo,abs(Y13));
xlabel('f/f0');
ylabel('Y21 magnitude-IDT')
```

```
subplot(414)
plot(f/fo,abs(Y33));
xlabel('f/f0');
ylabel('Y22 magnitude-IDT')
%----------------------------------------
de=[1 0 0 ;0 1 0 ; 0 0 1];
%M=det(de+Y);
M=(1+Y33).*((1+Y11).*(1+Y22)-(Y12.*Y21))-Y23.*(Y32.*(1+Y11)-(Y12.*Y31))-Y13.*(Y31.*↙
(1-Y22)-(Y21.*Y32));
%-----------------------------------
% S paramters calculation
%S=de-2*Y.*inv(de+Y);
S11=(1./M).*((1+Y33).*(1-power(Y11,2)+power(Y12,2))+(2*power(Y13,2).*(Y11+Y12)));
S22=S11;
S12=(-2./M).*(Y12.*((1+Y33)+power(Y13,2)));
S21=S12;
S13=(-2./M).*(Y13.*(1+Y11+Y12));
S31=S13;
S23=-S13;
S32=-S13;
S33=(1./M).*((1-Y33).*(power((1+Y11),2)-power(Y12,2))+2.*power(Y13,2).*(1+Y11+Y12));
%-----------------------------------
% S paramter plotting vs frequency in dB
%magdb=10*log10(abs(S21));
figure(2);
subplot(411)
plot(f/fo,20*log10(abs(S11)));
xlabel('f/f0');
ylabel('S11 magnitude dB-IDT')
subplot(412)
plot(f/fo,20*log10(abs(S12)));
xlabel('f/f0');
ylabel('S12 magnitude dB -IDT')
subplot(413)
plot(f/fo,20*log10(abs(S13)));
xlabel('f/f0');
ylabel('S21 magnitude db-IDT')
subplot(414)
plot(f/fo,20*log10(abs(S33)));
xlabel('f/f0');
ylabel('S22 magnitude dB-IDT')
%----------------------------------------------------------------------
%----------------------------------------------------------------------
% ABCD Matrix for IDT
x=Np*pi*((f-fo)/fo);
A=((2.*x)-1i)./(1i*4*Np);
B=(1./Go).*(A);
C=(pi.*f*Cs.*x)-(4*Np.*Go)-1i*((0.5*pi.*f*Cs)+((4*Np.*Go)./((2.*x)-1i)));
D=(pi*f*Cs*Ro.*x)-(4*Np)-(1i*0.5*pi*f*Cs*Ro);
Ain=A;
Bin=B;
Cin=C;
Din=D;
Aout=Din;
Bout=Bin;
```

```
Cout=Cin;
Dout=Ain;
check=(A.*D)-(B.*C);        % check   is equal to 1
%-------------------------------------------------------------------
%--------------------------------------------------------------------
 %propagation path ECM [ABCD]
 theta=(pi.*f*l)./(vsaw);
 Ap=cos(2.*theta);
 Dp=Ap;
 Bp=1i*sin(2.*theta);
 Cp=Bp;
 %-----------------------------------------------------------------

 %------------------------------------------------------------------
 % Delay line IDT-Prropagation path - IDT

 % [ABCD]IDR-in --->[ABCD]path --->[ABCD]IDT-out

 % [ABCD] of delay line

Dev=[Ain Bin;Cin Din].*[Ap Bp;Cp Dp].*[Aout Bout;Cin Dout];

%convert ABCD matrix to S-matrix of Delay line
for z =1:1:2001
 DDev=[Ain(z) Bin(z);Cin(z) Din(z)].*[Ap(z) Bp(z);Cp(z) Dp(z)].*[Aout(z) Bout(z);Cin↙
(z) Dout(z)];

SDev=abcd2s(DDev);
DS11(z)=SDev(1,1);
DS12(z)=SDev(1,2);
DS21(z)=SDev(2,1);
DS22(z)=SDev(2,2);

end

SS11=ifft(DS11);
SS12=ifft(DS12);
SS21=ifft(DS21);
SS22=ifft(DS22);

figure(3);
subplot(411);
plot(f/fo,20*log10(DS11));
xlabel('f/f0');
ylabel('S11 magnitude dB delayline')
subplot(412);
plot(f/fo,20*log10(DS12));
xlabel('f/f0');
ylabel('S12 magnitude dB delayline')
subplot(413);
plot(f/fo,20*log10(DS21));
xlabel('f/f0');
ylabel('S21 magnitude dB delayline')
subplot(414);
plot(f/fo,20*log10(DS22));
```

```
xlabel('f/f0');
ylabel('S22 magnitude dB delayline')
%-----------------------------------------------------------------
% figure(10);
% plot(f,20*log10((SDev(1,2))));
%  figure(11);
%  bode(DS11,f);
%  figure(12);
%  bode(DS12,f);

%------------------------------------------------------------------
%For Tag 1-IDT , propagation path1, R1 , propagation path 2, R2
L1=wavlength*1000; % 1 uS;
L2=wavlength*500; % 1.5 uS;

            %Propagation path 1
theta1=(pi.*f*L1)./(vsaw);
Ap1=cos(2.*theta1);
Dp1=Ap1;
Bp1=1i*sin(2.*theta1);
Cp1=Bp1;
            %Propagation path 2
theta2=(pi.*f*L2)./(vsaw);
Ap2=cos(2.*theta2);
Dp2=Ap2;
Bp2=1i*sin(2.*theta2);
Cp2=Bp2;

    % Refelctor can be assumed IDT without electrical port

    % R1 ABCD matrix
Np1=10;

% %-----------------------------------
 % Y paramters calculation
 for n=1:1:2000
alphaR1=(pi*n)/(2*fo);
R1Y11=-1i*Go*cot(4*Np1*alphaR1);
R1Y12=(1i*Go)./(sin(4*Np1*alphaR1));
R1Y13=0;
R1Y33=0;
R1Y22=R1Y11;
R1Y21=R1Y12;
R1Y31=R1Y13;
R1Y23=-R1Y13;
R1Y32=-R1Y13;

y_params = [R1Y11,R1Y12; R1Y21,R1Y22];
%Convert to ABCD-parameters
abcd_params = y2abcd(y_params);
R1A(n)=abcd_params(1,1);
R1B(n)=abcd_params(1,2);
R1C(n)=abcd_params(2,1);
R1D(n)=abcd_params(2,2);
 end
```

```
R1Ain=R1A;
R1Bin=R1B;
R1Cin=R1C;
R1Din=R1D;
R1Aout=R1Din;
R1Bout=R1Bin;
R1Cout=R1Cin;
R1Dout=R1Ain;

%ABCD of IDT- P1- R1


DevR1=[Ain Bin;Cin Din].*[Ap1 Bp1;Cp1 Dp1].*[R1Aout R1Bout;R1Cin R1Dout];

%---------------------------------------------------------------------------
%convert ABCD matrix to S-matrix of tag


for z =1:1:2001
 DDevR1=[Ain(z) Bin(z);Cin(z) Din(z)].*[Ap1(z) Bp1(z);Cp1(z) Dp1(z)].*[R1Aout(z)↙
R1Bout(z);R1Cin(z) R1Dout(z)];

SDevR1=abcd2s(DDevR1);
DS11R1(z)=SDevR1(1,1);
DS12R1(z)=SDevR1(1,2);
DS21R1(z)=SDevR1(2,1);
DS22R1(z)=SDevR1(2,2);
end

R1SS11=ifft(DS11R1);
R1SS12=ifft(DS12R1);
R1SS21=ifft(DS21R1);
R1SS22=ifft(DS22R1);



figure(4);
subplot(411);
plot(f/fo,20*log10(DS11R1));
xlabel('f/f0');
ylabel('S11 magnitude dB R1')
subplot(412);
plot(f/fo,20*log10(DS12R1));
xlabel('f/f0');
ylabel('S12 magnitude dB R1')
subplot(413);
plot(f/fo,20*log10(DS21R1));
xlabel('f/f0');
ylabel('S21 magnitude dB R1')
subplot(414);
plot(f/fo,20*log10(DS22R1));
xlabel('f/f0');
ylabel('S22 magnitude dB R1')
```

```
%-----------------------------------------------------------------
 % IDT-P1-R1-P2-R2
DevR2=[Ain Bin;Cin Din].*[Ap1 Bp1;Cp1 Dp1].*[R1Aout R1Bout;R1Cin R1Dout].*[Ap2 Bp2;↙
Cp2 Dp2].*[R1Aout R1Bout;R1Cin R1Dout];

%convert ABCD matrix to S-matrix of tag

%convert ABCD matrix to S-matrix of Delay line
for z =1:1:2001
 DDevR2=[Ain(z) Bin(z);Cin(z) Din(z)].*[Ap1(z) Bp1(z);Cp1(z) Dp1(z)].*[R1Aout(z)↙
R1Bout(z);R1Cin(z) R1Dout(z)].*[Ap2(z) Bp2(z);Cp2(z) Dp2(z)].*[R1Aout(z) R1Bout(z);↙
R1Cin(z) R1Dout(z)];

SDevR2=abcd2s(DDevR2);
DS11R2(z)=SDevR2(1,1);
DS12R2(z)=SDevR2(1,2);
DS21R2(z)=SDevR2(2,1);
DS22R2(z)=SDevR2(2,2);
end

 R2SS11=ifft(DS11R2);
 R2SS12=ifft(DS12R2);
 R2SS21=ifft(DS21R2);
 R2SS22=ifft(DS22R2);



figure(5);
subplot(411);
plot(f/fo,20*log10(DS11R2));
xlabel('f/f0');
ylabel('S11 magnitude dB R2')
subplot(412);
plot(f/fo,20*log10(DS12R2));
xlabel('f/f0');
ylabel('S12 magnitude dB R2')
subplot(413);
plot(f/fo,20*log10(DS21R2));
xlabel('f/f0');
ylabel('S21 magnitude dB R2')
subplot(414);
plot(f/fo,20*log10(DS22R2));
xlabel('f/f0');
ylabel('S22 magnitude dB R2')
%↙
-------------------------------------------------------------------------------------↙
----

% time domain transformation trial 1
% require exciting the IDT

% figure(6);
% subplot(411);
% plot(1./f,SS11);
% subplot(412);
```

```
% plot(1./f,SS12);
% subplot(413);
% plot(1./f,SS21);
% subplot(414);
% plot(1./f,SS22);
%
% figure(7);
% subplot(411);
% plot(1./f,R1SS11);
% subplot(412);
% plot(1./f,R1SS12);
% subplot(413);
% plot(1./f,R1SS21);
% subplot(414);
% plot(1./f,R1SS22);
%
% figure(8);
% subplot(411);
% plot(1./f,R2SS11);
% subplot(412);
% plot(1./f,R2SS12);
% subplot(413);
% plot(1./f,R2SS21);
% subplot(414);
% plot(1./f,R2SS22);
```

B. Appendix II: COM ECM Matlab Code


```
% COM IDT equivlent Circuit
%--------------------------------
% Device Specification
f=0:2000;
BW=26;
fo=915;
pi=3.1416;
Rin=50;
w=2*pi*f;
%--------------------------------
% Material properties
vsaw=3978;      % need to change for ALN
wavlength=vsaw/fo;
%--------------------------------
% IDT Specs.
width=wavlength/4;
spacing=width;
L=wavlength;
N=70;
%--------------------------------
% Material properties
K2=4.5/100;
Cs=4.6E-10;      % 4.6 pF/Cm for LiNbO3
Ct=Cs*N;
K11=0;      %coupling coeffiecient form Piezoelectric perturbation
K12=0.0000001;      %coupling coeffiecient form Mechanical perturbation
zeta= 2;     %Constant associated with convention from Electrical to SAW
Ha=(1/Rin)*(1/(2*fo*Cs*N))*((4*K2*N)/((4*K2*N*4*K2*N)+(pi*pi)));
%-------------------------------------------------------------------
% COM par
k=w/vsaw;
ko=(2*pi)/L;
del=k-ko;
B=sqrt(power((del+K11),2)-power(K12,2));
p=(B-del-K11)/K12;
q=1./(del+K11+K12);
Zo=(1-p)/(1+p);
theta=(B*N*L)/2;
phi=2i*N*L*K2;
%----------------------------------------------------------------------
% circuit schematic paramters
%IDT
imped1=2i*theta.*Zo;
imped2=1i*Zo.*sin(2*theta);
imped3=(-1i.*Zo)./tan(theta);
%propagation path
imped4=1i*conj(Zo).*sin(2*conj(theta));
imped5=(-1i*conj(Zo))./tan(conj(theta));


% figure(1);
% subplot(411)
% plot(f,abs(phi));
% subplot(412)
% plot(f,abs(theta));
```

```
% subplot(413);
% plot(f,abs(Zo));
% subplot(414)
% plot(f,real(imped1));
figure(1);
subplot(511)
plot(f/fo,real(imped1));
xlabel('f/fo');
ylabel('impedance 1 real');
subplot(512)
plot(f/fo,real(imped2));
xlabel('f/fo');
ylabel('impedance 2 real');
subplot(513)
plot(f/fo,real(imped3));
xlabel('f/fo');
ylabel('impedance 3 real');
subplot(514)
plot(f/fo,real(imped4));
xlabel('f/fo');
ylabel('impedance 4 real');
subplot(515)
plot(f/fo,real(imped5));
xlabel('f/fo');
ylabel('impedance 5 real');

figure(2);
subplot(511)
plot(f/fo,imag(imped1));
xlabel('f/fo');
ylabel('impedance 1 imag');
subplot(512)
plot(f/fo,imag(imped2));
xlabel('f/fo');
ylabel('impedance 2 imag');
subplot(513)
plot(f/fo,imag(imped3));
xlabel('f/fo');
ylabel('impedance 3 imag');
subplot(514)
plot(f/fo,imag(imped4));
xlabel('f/fo');
ylabel('impedance 4 imag');
subplot(515)
plot(f/fo,imag(imped5));
xlabel('f/fo');
ylabel('impedance 5 imag');
```

C. Appendix III: Simple delay line (input IDT-propagation path-output IDT)

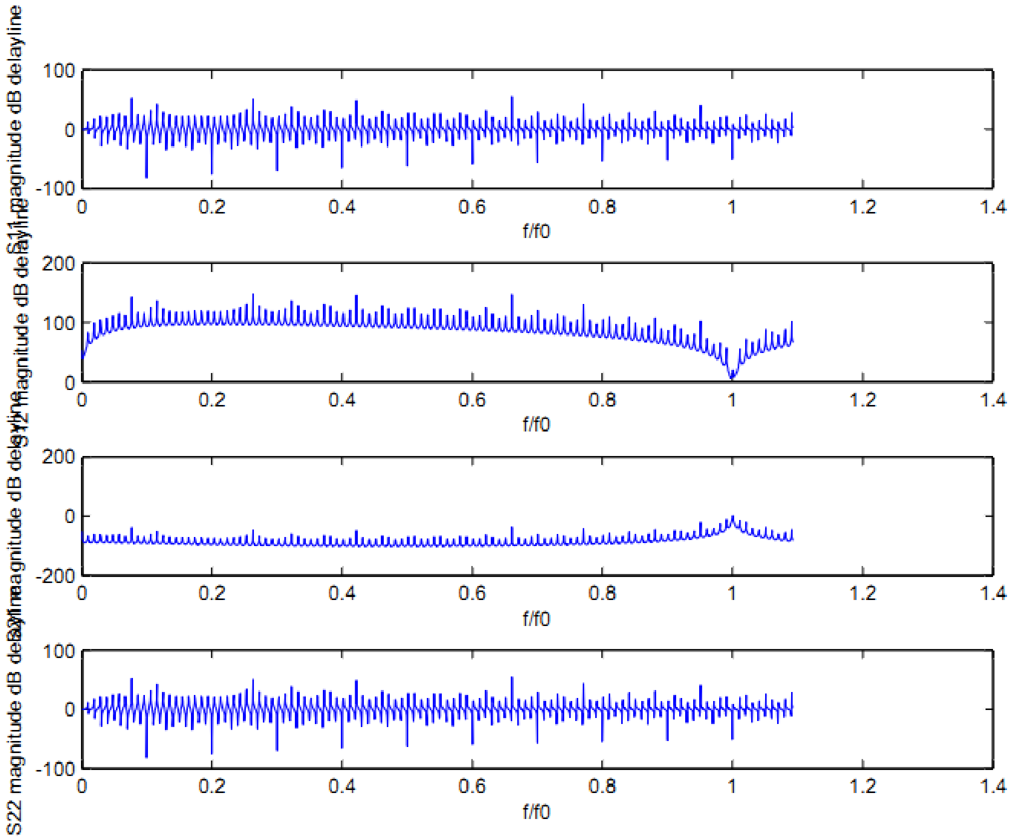

D. Appendix IV: Simple tag (input ID- propagation path- reflector)

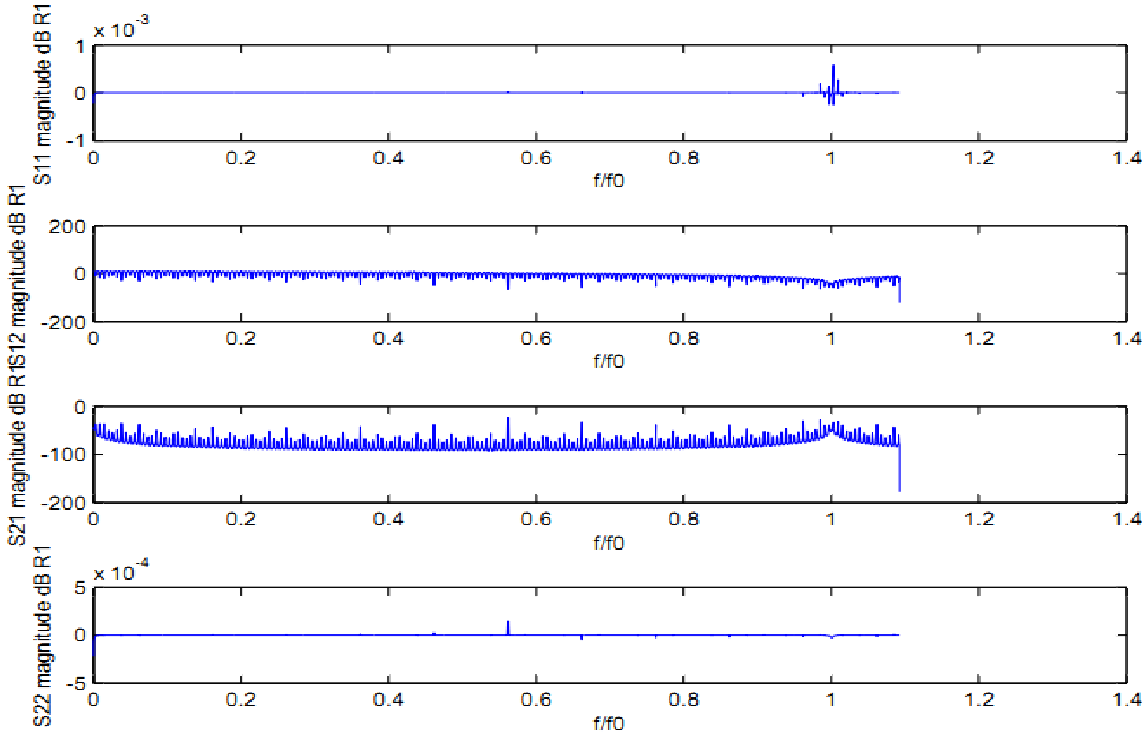

E. Appendix V: Simple tag (input ID- propagation path 1- reflector1- propagation path 2- reflector 2)

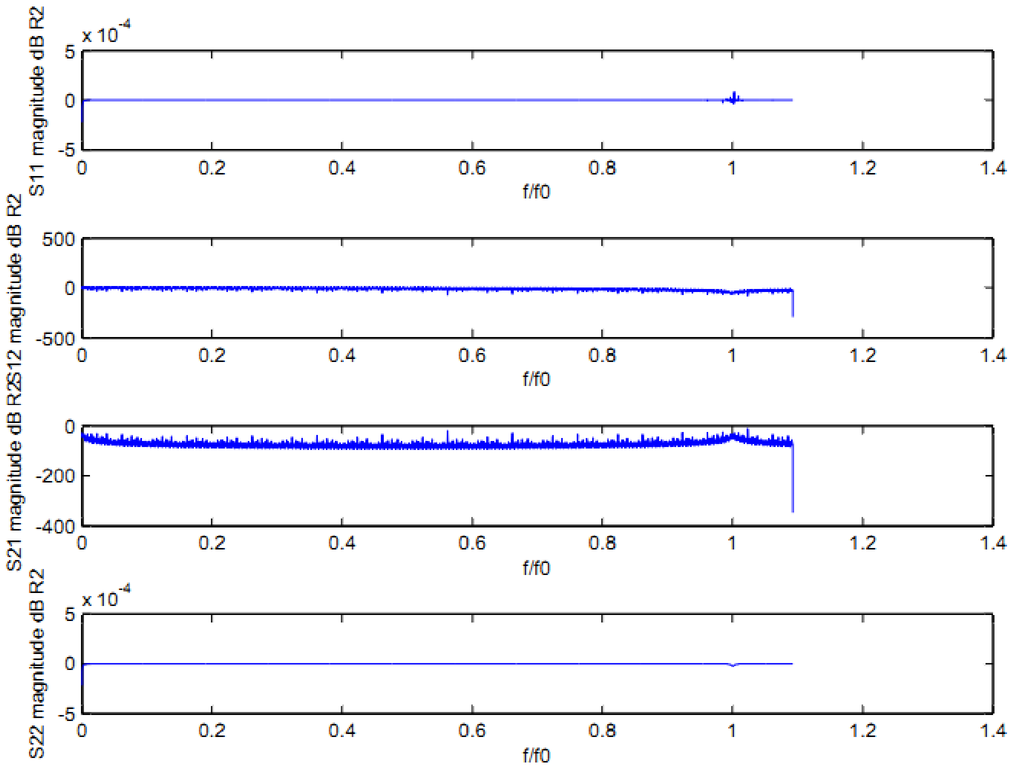

F. Appendix VI: COM impedance parameter calculations

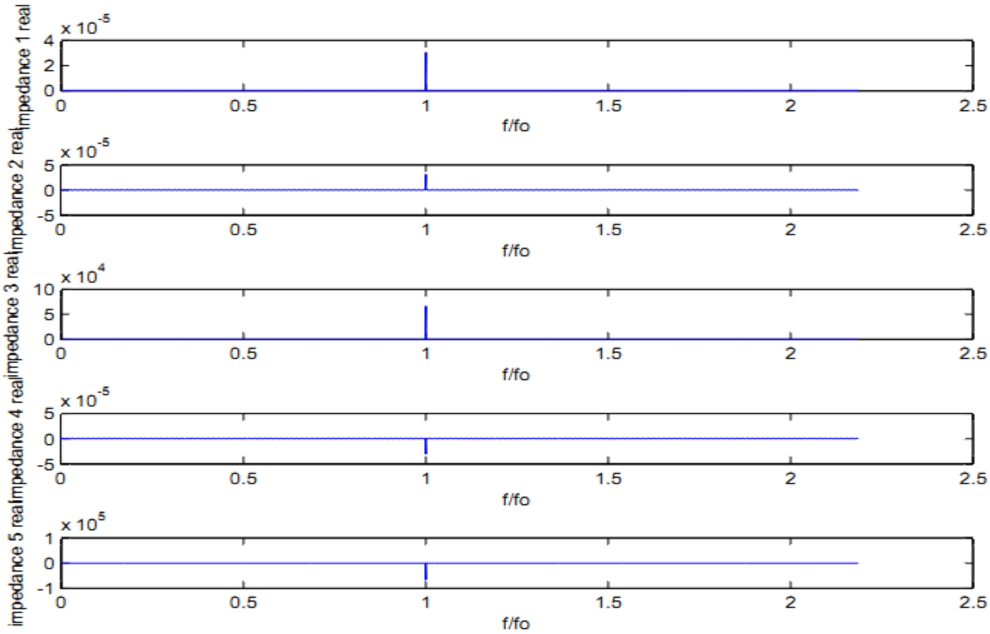

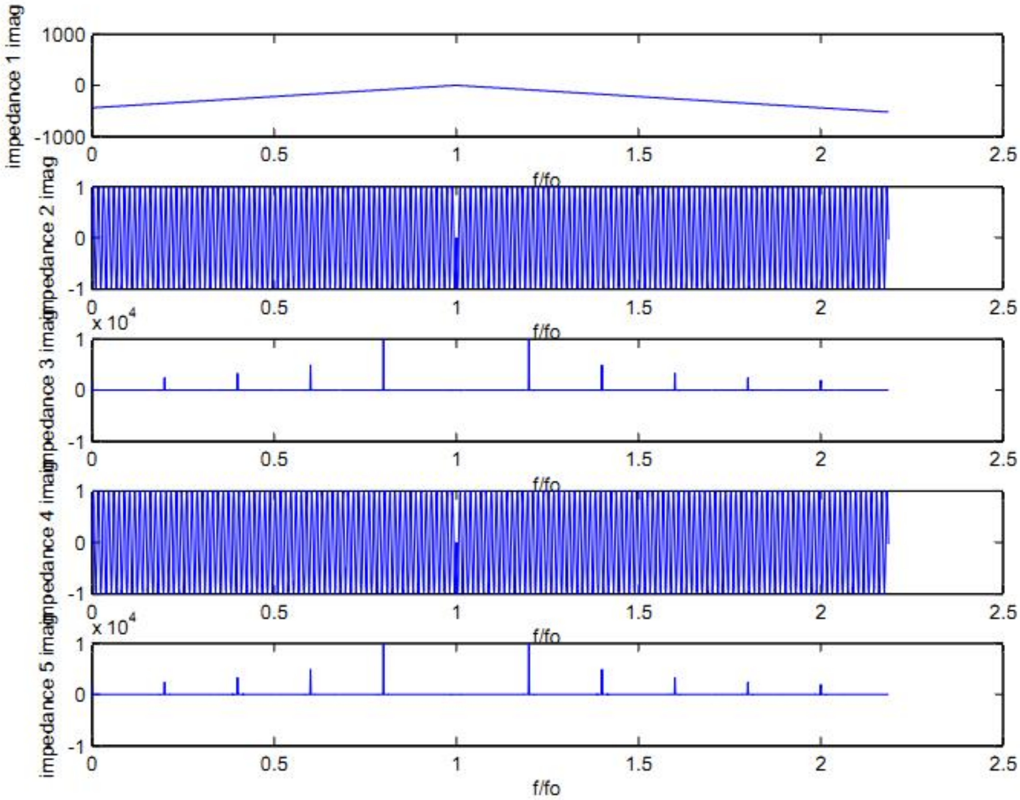

G. Appendix V: Stack thickness of SAW delay lines

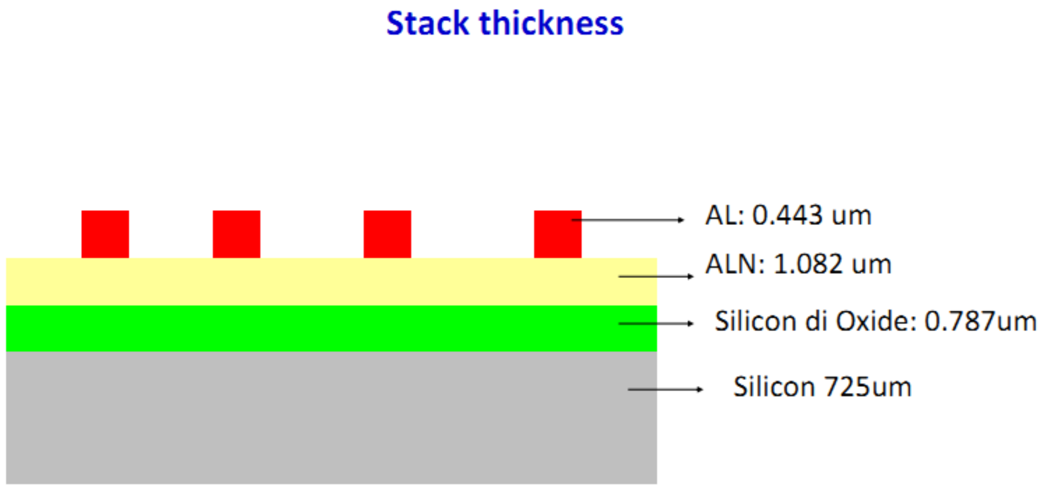

H. Appendix VI: Expected SAW velocity Model 1

```
%-------------------------------------------------------------------------
%Device wavelength
wavelength=20E-6;    % wavelength of devices are 12,8,6,4 um
%-------------------------------------------------------------------------
% device thickness profile
%-------------------------------------------------------------------------
AlNh=0E-6:0.1E-6:40E-6;
SiO2h=0.787E-6;
Sih=725E-6;                 % Sih=725E-6;
%-------------------------------------------------------------------------
%Material properties
%Source:Monolithic integrated SAW filter based on AlN for high-frequency
%applications (Source B)
%-------------------------------------------------------------------------
AlNden=3230;        %kg/M^3
SiO2den=2200;       %kg/M^3
Siden=2330;         %kg/M^3
%-------------------------------------------------------------------------
%-------------------------------------------------------------------------
%SAW velocity estimation based on source(C) FEM simulation:Design and
%realization of SAW pressure sensor using Aluminum % Nitride  By :Trang HOANG
%------------------------------------------------------------------------
KhAlN=(AlNh)./wavelength;
KhSiO2=(SiO2h)./wavelength;
KhSi=(wavelength-SiO2h)./wavelength;
%-------------------------------------------------------------------------
% Using FEM plot we estmate the SAW velcoity based on KhAlN and KhSiO2
%-------------------------------------------------------------------------
% ------------------------------------------------------------------------
% Model used source :Modelling and wave velocity calculation of multilayer
% structure SAW sensors (Source A)
% by :Dejan V.Tos?ic
%-------------------------------------------------------------------------
%-->v
%------------Zu---------Zd----
%                             |
%  Fi                         |
%                             Zb
%                             |
%-----------------------------|
%-------------------------------------------------------------------------
vsi=4900;         %Saw velocity in silicon alone (source A)
vSiO2=3750;
vAlN=5760;
v1=((vsi*Siden*KhSi)+(vSiO2*SiO2den*KhSiO2))./((AlNden.*KhAlN)+(SiO2den*KhSiC
v2=((vSiO2*SiO2den*(KhSiO2))+(vAlN*AlNden*KhAlN))./((AlNden.*KhAlN)+(SiO2den*
v3=((vAlN*AlNden*KhAlN))./((AlNden.*KhAlN));

figure(1);
plot(KhAlN,[v1;v2;v3]);
```